Contributions to Mineralogy and Petrology (2020) 175:28
https://doi.org/10.1007/s00410-020-1666-3

ORIGINAL PAPER

Petrogenesis of the Gifford Creek Carbonatite Complex, Western Australia

Paul Slezak[1,2] · **Carl Spandler**[1]

Received: 13 September 2019 / Accepted: 17 February 2020 / Published online: 3 March 2020

Abstract

The 1370 Ma Gifford Creek Carbonatite Complex (GCCC) comprises a diverse suite of alkaline dyke and sill complexes that cover an area of ~ 250 km^2 in the Gascoyne Province, Western Australia. Most carbonatite types are interpreted to be related products of fractional crystallisation, with calcite carbonatites representing cumulate rocks and dolomite carbonatites representing crystallised products of the derivative liquids. Genetic relationships between these carbonatites and other alkaline igneous units are less clear. The ankerite–siderite carbonatites and magnetite-biotite dykes are likely of related magmatic origin as both have distinctly high LREE and low HFSE contents. The ankerite–siderite carbonatites have mantle-like $\delta^{13}C$ isotope values of − 6.1 to − 7.1‰ and similar geochemistry to other known magmatic ferrocarbonatites. Silica-rich alkaline veins found near the centre of the complex have trace element signatures that are antithetic to the magnetite–biotite dykes, so these veins are interpreted to represent products of alkali- and F-rich magmatic-hydrothermal fluids exsolved from the magnetite–biotite dykes during their emplacement. Carbon, O, Sr, and Nd isotope data are consistent with an enriched mantle source for the origin of the GCCC, with mantle enrichment likely caused by plate convergence processes associated with the c. 2.0 Ga Glenburgh Orogeny. There is no evidence to link mantle plume activity with formation of the GCCC; rather, alkaline magmatism is interpreted to result from low degree melting of the metasomatised mantle during reactivation of the crustal suture zone at 1370 Ma. The carbonatitic magmas utilised the Lyons River Fault to traverse the crust to be emplaced as the GCCC. Post magmatic alteration has variably modified the O and Sr isotope compositions of carbonates from these rocks. We therefore appeal for careful evaluation of isotopic data from ancient carbonatites, as isotopic resetting may be more common than currently recognised.

Keywords Carbonatite · Gifford Creek Carbonatite Complex · Mesoproterozoic · Radiogenic isotopes · Stable isotopes

Introduction

Carbonatites are relatively uncommon igneous rocks that are important hosts for rare metal mineralisation including the rare earth elements (REE) and high field strength elements (HFSE; Chakhmouradian and Williams 2004; Wall and Zaitsev 2004). Carbonatite complexes also provide a record of melting from enriched mantle domains through time and can be used to infer past episodes of continental rifting, intra-continental magmatism (Slezak and Spandler 2019), or mantle plume activity (Pirajno 2015). They commonly form plug-like or brecciated intrusive bodies but can also occur as hypabyssal dykes and/or sills under extensional stress regimes (Keller 1989). While most carbonatites are Ca- and/or Mg-rich, forming calcite and dolomite carbonatites, a relatively minor group is rich in Fe and form ankerite and/or siderite carbonatites. These ferrocarbonatites are

Communicated by Steven Reddy.

Electronic supplementary material The online version of this article (https://doi.org/10.1007/s00410-020-1666-3) contains supplementary material, which is available to authorized users.

✉ Paul Slezak
paul.slezak@ucd.ie

[1] Department of Geoscience, College of Science and Engineering, James Cook University, Townsville, QLD 4811, Australia

[2] Present Address: School of Earth Sciences, University College Dublin, Belfield, Dublin 4, Ireland

often associated with REE mineralisation and are commonly considered to be late stage and hydrothermal in origin (Le Bas 1989; Zaitsev et al. 2004), although some ferrocarbonatites, such as the Swartbooisdrif and Central Tuva ferrocarbonatites, are interpreted to be magmatic in origin (Drüppel et al. 2004; Prokopyev et al. 2016).

Carbonatites of all types are also often associated with a wide variety of other rock types including lamprophyres, kimberlites, pyroxenites, peridotites, syenites, melilites, nephelinites, phonolites, and phoscorites (Woolley and Kjarsgaard 2008). The Gifford Creek Carbonatite Complex (GCCC), Gascoyne Province, Western Australia contains a diverse range alkaline magmatic and hydrothermal phases, many of which are prospective for LREE mineralisation, over an area of ~ 250 km^2. Despite the economic potential and the diversity of rock types in the complex (including some first described here), the GCCC has not previously been subject to extensive geological study. This paper outlines the petrology and geochemistry of the GCCC, and, in particular, aims to establish the origin and evolution of various rock units of the complex. These relationships are germane to understanding the evolution carbonatite-related magmatism, as well as regional tectonic and geologic controls on rare metal mineralisation in these rock systems.

Geology of the Gifford Creek Carbonatite Complex

The GCCC lies within the Gascoyne Province (Fig. 1), which sutures Archean-aged rocks of the Pilbara Craton, Glenburgh Terrane, and Yilgarn Craton to form the Western Australia Craton. The Gascoyne Province comprises a variety of Mesoproterozoic granitoids, granitic and metasedimentary gneisses, and metasedimentary rocks that have undergone a ~ 1 b.y. history of terrane assembly and reworking, resulting in multiple, fault-bounded tectonic zones (Fig. 1; Sheppard et al. 2010).

The GCCC is located in the northeastern region of the Mangaroon Zone (Fig. 1; see Sheppard et al. 2005), which comprises the c. 1760–1680 Ma Pooranoo Metamorphics (mainly pelitic to arkosic schists, gneisses, and migmatites) as well as the granitic rocks of the c. 1680–1620 Ma Durlacher Supersuite (Pearson et al. 1996; Sheppard et al. 2005). These rock units are unconformably overlain by 1673–1455 Ma Edmund Group sedimentary rocks (Martin and Thorne 2004).

The GCCC was emplaced c. 1370 Ma into the previously described host rocks based on radiometric dating of a variety of rock types from the complex (Zi et al. 2017; Slezak and Spandler 2019). The GCCC is bounded in the south by the northwest–southeast striking Lyons River Fault, which represents the crustal suture between the Archean–Neoarchean

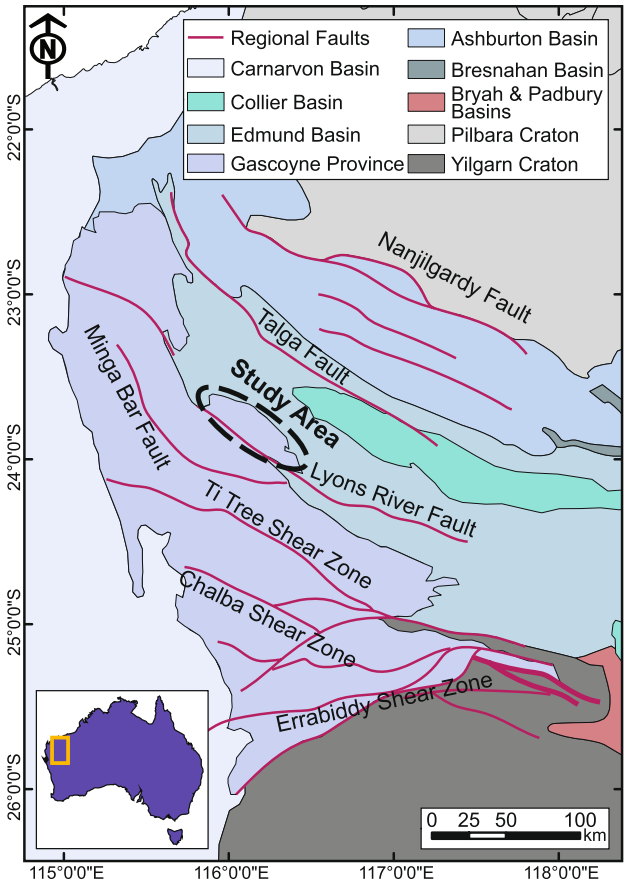

Fig. 1 Regional tectonic map of the Gascoyne Province with major bounding structures. Note that the Ti Tree Shear Zone and Chalba Shear Zone are faults and not tectonic zones. The GCCC is located in the lobate feature on the margin of the Mangaroon Zone, constrained by the Lyons River Fault in the southwest and the Edmund Basin in the northeast

Glenburgh Terrane and the Archean Pilbara Craton (Johnson et al. 2013). The Bald Hill Lineament runs subparallel to the Lyons River Fault and separates massive, dextrally sheared granites in the northern region from the complex assortment of schists, granites, and alkaline dykes in the southern region (Fig. 2; Pearson 1996; Pearson et al. 1996). The area between the Bald Hill Lineament and the Lyons River Fault contains most of the exposed alkaline rocks of the GCCC.

The GCCC consists of several different rock types, some of which have been previously defined, creating ambiguity in their identification. The Yangibana Ironstones were first described as such by Gellatly (1975) and the name is still often used. The swarm of SE-trending rocks near the Lyons River Fault (Fig. 2) have historically been called the Lyons River Sills. These units were described as ultrabasic sills by Pearson (1996) and Pearson et al. (1996), and as ferrocarbonatites by Pirajno et al. (2014). The present study documents previously undescribed rock units in the GCCC and re-evaluates previously documented units (e.g.,

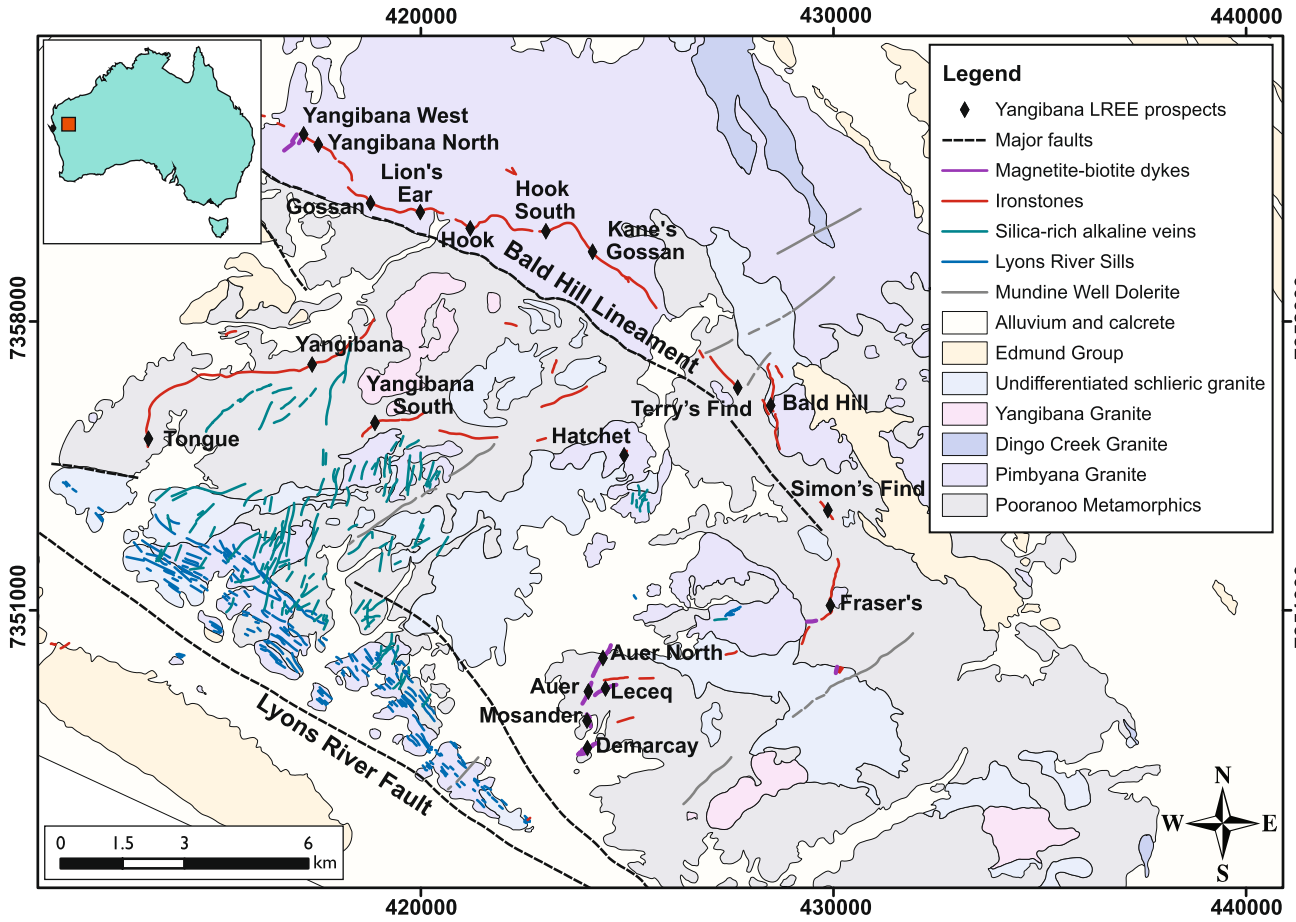

Fig. 2 District-scale map of the GCCC showing the distribution of the alkaline dyke units, their host rocks, and major mineral deposits that comprise the Yangibana LREE district (modified after Slezak et al. 2018)

the Lyons River Sills). We identify four primary rock types: (1) dolomite and calcite carbonatites—also known as the Lyons River Sills—(Fig. 3a, b); (2) ankerite–siderite carbonatites (Fig. 3c); (3) magnetite–biotite dykes (Fig. 3d); and (4) silica-rich alkaline veins (Fig. 3e). In addition, there are three rock types related to alteration: (1) the Yangibana Ironstones, which host LREE mineralisation of economic interest; (2) fenites (Fig. 3f); and (3) glimmerites (Fig. 3g). The latter two phases are altered wall rocks created through interaction with alkaline, carbonatite-related fluids.

Lyons River Sills

The Lyons River Sills occur in the southern region of the GCCC mainly as a swarm of dykes and sills, striking subparallel to the Lyons River Fault (i.e., ~ 130°–150°) and dipping 30°–60° SW, but they have also been found in the northeast near the Fraser's deposit (Fig. 2). The Lyons River Sills range from 10 cm to 1.5 m in width and are continuous for tens to several hundreds of metres, although individual dykes/sills are rarely traceable for longer distances due to offset by small faults or cover by vegetation and surficial sediments. The Lyons River Sills are primarily of dolomite carbonatites (Fig. 3a) with minor calcite carbonatites (Fig. 3b). Weathered surfaces of both rock-types are buff to dark brown in colour (Fig. 3a, b), whereas fresh rock surfaces appear blue (Fig. 3b) to green in colour, depending on to the relative abundances of arfvedsonite (blue) and aegirine (green).

Dolomite carbonatites

The dolomite carbonatites are composed of 50–65% Fe-bearing dolomite and 10–30% arfvedsonite and aegirine, with minor amounts of biotite, magnetite, ilmenite, and apatite as well as trace amounts of monazite, zircon, pyrite, and chalcopyrite. Textural features of the carbonatite sills are heterogeneous, varying between porphyritic, equigranular, and seriate textural varieties (Fig. 4a).

Relative proportions of aegirine and arfvedsonite vary considerably, even within the same dyke. Textural relations indicate that arfvedsonite (100–500 µm) formed

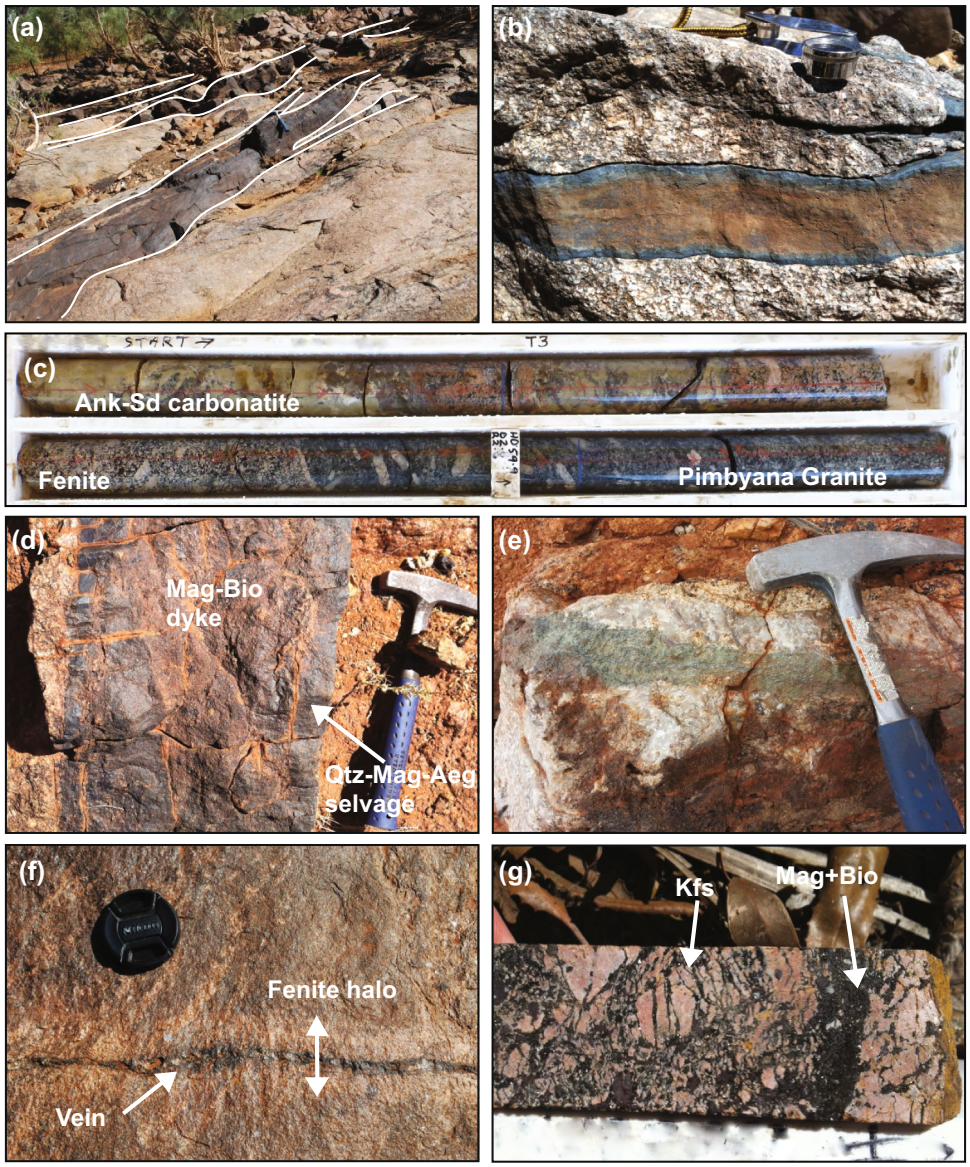

Fig. 3 Field photos of the various alkaline intrusive units of the GCCC. **a** Lyons River Sills dolomite carbonatite with dark brown weathering patina. **b** Lyons River Sills calcite carbonatite with blue, Mg-rich arfvedsonite margins. **c** Coarse-grained ankerite–siderite carbonatite dyke found in drill hole YN49 at Yangibana North with pink, fenite alteration of the porphyritic Pimbyana Granite host rock. **d** Coarse-grained magnetite–biotite dyke at Demarcay with fine-grained margins similar to the silica-rich alkaline veins in **e**. **e** Aegirine-, HFSE- and silica-rich alkaline vein in a larger quartz vein hosted in the Pimbyana Granite. The dyke is located in the swarm south of Yangibana South in Fig. 2. **f** Fenite halo around an alkaline amphibole–dolomite veinlet that emanates from a dolomite carbonatite parent dyke. **g** Fenitised granite cut by magnetite and biotite alteration selvages (i.e., glimmerites) from Yangibana West. *Aeg* aegirine, *Ank* ankerite, *Bio* biotite, *Kfs* potassium feldspar, *Mag* magnetite, *Qtz* quartz, *Sd* siderite

coincidently with dolomite, and, in the matrix of some samples, Mg-bearing biotite. Aegirine presents as 20 µm wide and up to 100 µm long euhedral needles that appear to overprint dolomite (Fig. 4b). Biotite forms laths and plates up to 300 µm across, and is most common in the equigranular-textured dolomite carbonatites and in the matrix of the porphyritic-textured carbonatites (Fig. 4a). It is intergrown with dolomite, but often has embayed or ragged crystal margins.

Magnetite (partly altered to hematite), ilmenite, and apatite typically occur as fine (20–150 µm) accessory phases distributed throughout in the dolomite carbonatites, although apatite abundance varies greatly and can display minor banding. Trace amounts of monazite and zircon are present as small (< 10–20 µm) crystals in apatite and dolomite, respectively.

Calcite carbonatites

The calcite carbonatites are composed of calcite, dolomite, arfvedsonite, apatite, and magnetite. Calcite is typically anhedral to subhedral and generally ranges in size from 50 to 100 µm, but it also presents as larger (up to 500 µm) crystals distributed in 1 mm diameter blebs and horizons within the dykes (Fig. 4c). Dolomite occurs as ~ 100 µm individual crystals, or as 1–3 mm crystal clots surrounded by calcite. The dolomite crystals often entrain small crystals of calcite. Contacts between calcite and dolomite are irregular and embayed for both individual crystals and the larger clots (Fig. 4c).

Apatite comprises between 5 and 20% of the calcite carbonatites and typically occurs as 30–100 µm ovoid grains concentrated in horizons (0.5–10 mm thick) or as

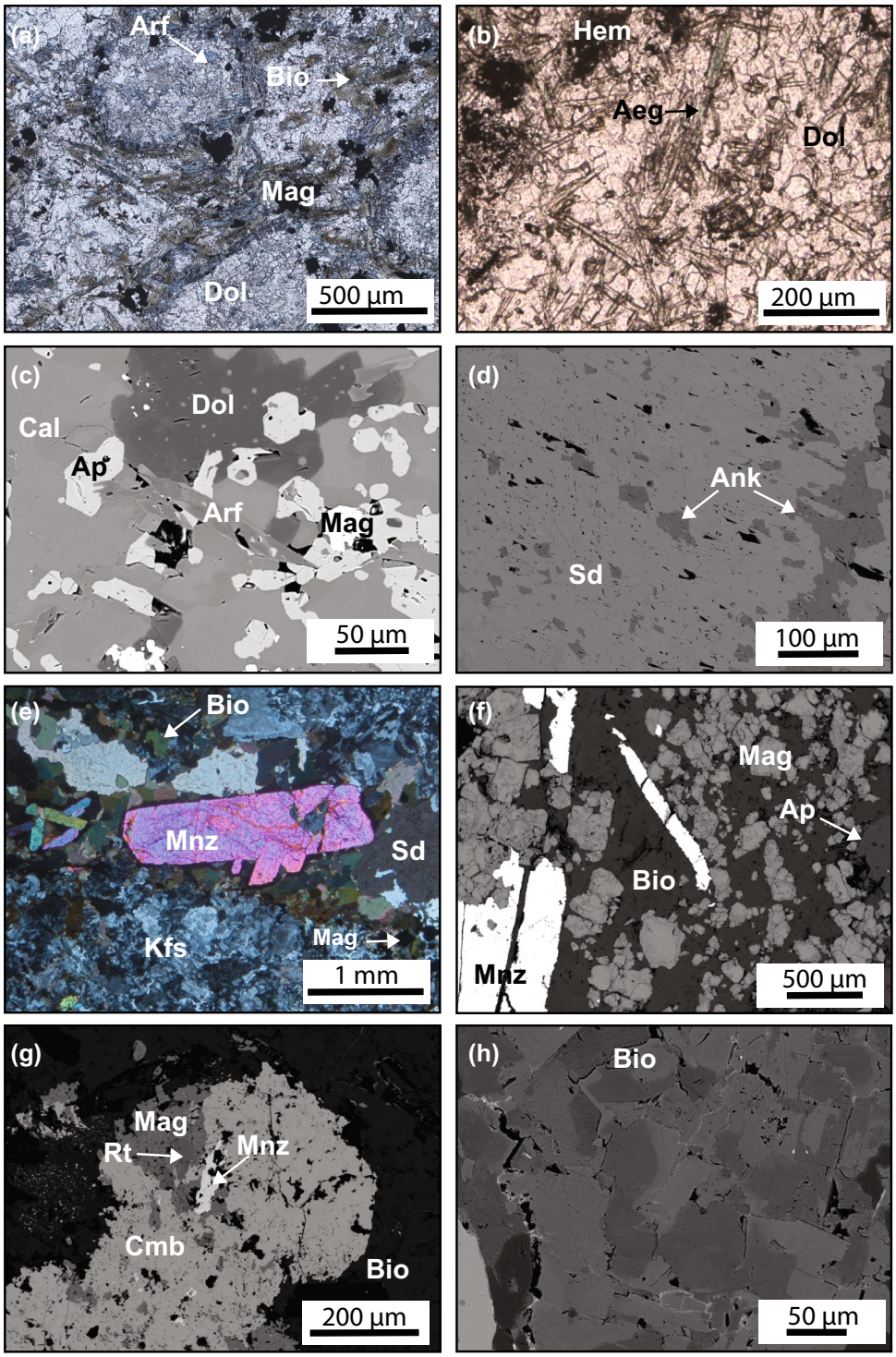

Fig. 4 Thin section photos of the main rock types of the GCCC. *PPL* plane polarised light, *XPL* cross-polarised light, *BSE* backscattered electron. **a** PPL image of dolomite carbonatite composed of rounded dolomite and arfvedsonite clasts in matrix of dolomite, biotite, magnetite, and arfvedsonite. **b** PPL image of dolomite carbonatite with aegirine needles. **c** BSE image of calcite carbonatite with dolomite inclusions. Small specs of calcite are also within the dolomite crystals. **d** BSE image of ankerite and siderite intergrowth in an ankerite–siderite carbonatite sample. **e** XPL image of ankerite–siderite carbonatite veinlet containing monazite. The veinlet contact with granite host rock is composed of biotite and magnetite. The granite has been fenitised to K-feldspar. **f** BSE image of magnetite–biotite dyke with large monazite crystals and magnetite clusters. **g** BSE image of a silica-rich alkaline vein with columbite with monazite, Ti-bearing magnetite, and Nb-bearing rutile. **h** BSE image of biotite from a Demarcay magnetite–biotite dyke with dark and light zonation. Cleavage planes can be observed passing uninterrupted through both zones. *Aeg* aegirine, *Ank* ankerite, *Ap* apatite, *Arf* arfvedsonite, *Bio* biotite, *Cal* calcite, *Cmb* columbite, *Dol* dolomite, *Hem* hematite, *Kfs* potassium feldspar, *Mag* magnetite, *Mnz* monazite, *Rt* rutile, *Sd* siderite

disseminated crystals. Many apatite grains contain small inclusions of carbonate minerals (Fig. 4c). Magnetite has the same occurrence in the calcite carbonatites as the dolomite carbonatites, but is more common where apatite is also present.

Arfvedsonite (7–10% of the rock) occurs as tabular grains, 100–200 µm in size, and shows slight zoning (Fig. 4c) that relates to variations in Ca and Fe contents (as determined by EDS). Arfvedsonite often contains small (~ 5–20 µm) apatite inclusions and, rarely, ~ 1 µm inclusions of magnetite.

Ankerite–siderite carbonatites

The ankerite–siderite carbonatites are presently only recognised from drill core as 5 cm to 1 m thick dykes cutting the Yangibana and Pimbyana granites (Fig. 3c) beneath the NW–SE trending ironstones subparallel to the Bald Hill Lineament. The ankerite–siderite carbonatites comprise siderite, ankerite, calcite, Fe-rich biotite, magnetite, monazite, apatite, and quartz. Siderite is usually > 2 mm in size and contains zones of smaller (20–200 µm) ankerite (Fig. 4d); however, the proportions of ankerite and siderite can vary considerably (Slezak et al. 2018). Calcite is only present in small quantities proximal to quartz. Quartz forms small domains (~ 1 cm) within carbonate minerals, occasionally entraining siderite and ankerite crystals. The contacts between quartz and carbonate minerals are often irregular and embayed. Monazite is present as euhedral laths ranging in size from 100 to 1000 µm and often occurs as grain clusters (Fig. 4e) within both the carbonate and quartz domains. Anhedral to subhedral apatite (200–500 µm in size) occurs proximal to monazite. In some samples, apatite crystals occur as aggregates up to 1 mm in diameter. Magnetite and biotite co-exist as euhedral crystals (50–250 µm in size), mainly along the contacts between the carbonate minerals and granitic host rock (Fig. 4e) as ~ 1–2 cm thick alteration selvages immediately adjacent to the ankerite–siderite carbonatites (Fig. 3g) and as anastomosing veinlets occurring within fenites. The biotite and magnetite crystals are large (50–200 µm) and often euhedral. Large (150–500 µm), dipyramid-shaped zircons with short prismatic faces are also present in the alteration selvages proximal to the ankerite–siderite carbonatites. These assemblages are analogous to glimmerites (Le Maitre 2002; Elliott et al. 2018).

Magnetite–biotite dykes

Steeply dipping dykes (Fig. 3d) and flat-lying sills composed largely of magnetite and biotite are located in the northwest corner near Yangibana North and Yangibana West (Fig. 2) and in the southeast region near Fraser's down to the Demarcay deposits (Fig. 2). These units (here termed magnetite–biotite dykes, but previously called phoscorites by Slezak et al. (2018)) trend northeast to southwest, are 10 cm to 1.5 m thick, and extend for tens to hundreds of metres at the surface. The contacts between the granite host rock and magnetite–biotite dykes are usually sharp, although some small injection veinlets of magnetite and biotite are present, occasionally forming crackle breccias in the host rock, proximal to the main body.

The magnetite–biotite dykes are black, equigranular intrusive units composed of magnetite, biotite, apatite, and monazite. Magnetite forms subhedral to euhedral crystals, up to 500 µm in size (Fig. 4f), contains patchy hematite alteration, and may contain inclusions of monazite. Most samples contain both apatite and monazite, but their relative abundances vary greatly, even within the same dyke. Platy biotite is present as 100–500 µm, subhedral to euhedral crystals (Fig. 4f), and sometimes presents as an interstitial phase to magnetite and apatite. Apatite forms anhedral to subhedral crystals 50–1500 µm in size (Fig. 4f) and often forms large clots, even aggregating together to create large pods (centimetres in size) within the magnetite–biotite dykes. Apatite ubiquitously hosts small, anhedral monazite inclusions (< 10 µm), and under cathodoluminescence (CL), it exhibits complex zonation (Slezak et al. 2018). Monazite is present in most samples and occurs as splayed clusters of large (up to 1 mm) euhedral crystals (Fig. 4f) or as small inclusions in apatite and magnetite. No carbonate minerals were observed in the magnetite–biotite dykes.

Silica-rich alkaline veins

The central region of the GCCC hosts a swarm of subvertical to vertical dipping silica-rich alkaline veins (Fig. 2) that have a strike orientation of between 000° and 020°; i.e., orthogonal to the Lyons River Sills. Although the veins occur in close proximity to the Lyons River Sills in the south-central area of the complex, direct field relationships between the two units have not been observed. The silica-rich alkaline veins are absent to the north of the Yangibana and Yangibana South mineral deposits (Fig. 2).

Individual veins range in width from 3 cm to 50 cm (Fig. 3e), but often extend for tens to several hundreds of metres and are spatially associated with quartz veins of similar orientations. The veins are variably green to beige in colour, often exhibit evidence of multiple fluid pulses, and are crosscut by quartz-filled tension gashes. The veins are composed of diverse assemblages and proportions of minerals, including phlogopite, aegirine, quartz, zircon, rutile, magnetite, columbite, arfvedsonite, and monazite. Phlogopite (100–500 µm in size) is anhedral to subhedral and has undergone partial alteration to Fe- oxides/hydroxides and aegirine along cleavage planes and crystal margins. Quartz is often present ~ 200 µm subhedral to anhedral crystals within the veins and also in cavities and in tensions gashes. Aegirine is present in the groundmass as 10–100 µm acicular crystals, crystal splays, or as an alteration product of phlogopite.

In some samples, zircon occurs in significant quantities, presenting as large, feathery clots up to 3 mm in diameter. More often, it presents as euhedral, dipyramids between 150 and 500 µm in size with shortened prismatic faces (Slezak and Spandler 2019). Columbite and rutile appear as anhedral phases (10–200 µm in size) associated with ~ (100 µm) anhedral to euhedral grains of Ti-bearing magnetite (Fig. 4g). Columbite also occurs as inclusions within the feathery to fibrous zircon clots. Rare monazite occurs as 50–200 µm

anhedral laths that are occasionally intergrown with the fine-grained, feathery zircon and/or columbite (Fig. 4g).

Yangibana Ironstones

The Yangibana Ironstones crop out across the GCCC (Fig. 2). These rocks are significant hosts for LREE mineralisation and are composed of fine-grained iron oxides, iron hydroxides, quartz, monazite, and rhabdophane (Pirajno et al. 2014; Slezak 2019). They have vuggy and/or botryoidal textures and often have weathered cavities resembling carbonate parallelepipeds. These rocks are alteration products and are not discussed further in this manuscript.

Fenites

All rock types are mantled by white to pink halos of fenitised granite and metasediments (e.g., fenites). The fenites are predominantly composed of potassium feldspar, and the extent of alteration is proportional to the size of the dyke, sill, or vein. Fenites are present in both schists of the Pooranoo Metamorphics and Edmund Group sedimentary rocks but are most obvious in the granitic rocks. In the fenitic alteration halos, plagioclase is pervasively altered to irregularly shaped potassium feldspar (20–300 µm) with tartan twinning. Quartz is present as fine-grained (~ 50 µm) crystals with recrystallised grain boundaries and undulose extinction. Apatite forms anhedral to subhedral crystals (up to 500 µm), many of which are zoned with REE-rich rims (Slezak et al. 2018). Monazite occurs as an interstitial phase filling in voids and fractures in potassium feldspar and quartz, and as small inclusions (~ 10 µm) in apatite.

Analytical methods

Samples collected for this study are from surface outcrops and diamond drill core. All samples were prepared as polished thin sections and initially examined using a Leica DMRXP optical microscope. Major and trace element compositions of minerals were determined at James Cook University by electron probe micro-analyser and laser ablation ICP-MS, respectively. Bulk rock analyses were completed by Bureau Veritas Commodities Canada Ltd. Oxygen, C, and Sr isotopes for carbonates were respectively measure by ThermoFisher DeltaV^{PLUS} isotope ratio mass spectrometer and Neptune MC-ICP-MS at James Cook University. Bulk rock Nd isotope ratios were determined by TIMS at the University of Adelaide. Full analytical details are presented in Supplementary Material 1.

Results

Mineral chemistry

Biotite-series chemistry

Biotite-series mica is present in nearly all of the alkaline igneous rocks in the GCCC and displays a patchy light and dark texture under BSE (Fig. 4h). The majority of mica contains intermediate Mg and Fe compositions along the annite–phlogopite solid solution series (Supplementary Material 5) and is therefore referred to as "biotite". In general, biotite with higher Mg content is associated with the Lyons River Sills, the magnetite-biotite dykes from the southeast GCCC, and the silica-rich alkaline veins (Supplementary Material 2; Supplementary Material 5), which are closest to tetraferriphlogopite in composition. Iron and Al contents of biotite are highest in the ankerite–siderite carbonatites and associated magnetite–biotite dykes (Supplementary Material 2; Supplementary Material 5). The darker BSE zones are Mg-rich and have higher F and Si, but lower Al and Cl contents (Supplementary Material 5 and Fig. 5a, b). The Ti and K contents are highest in biotite with high Fe/(Fe + Mg) (Fig. 5c, e).

Biotite analysed from the magnetite–biotite dykes has elevated Mn contents compared to Fe and Mg (Fig. 5f). Two samples from the northwestern and northern GCCC (YW61 and BH224) have biotite Mn values commensurate with the contents in biotite hosted in ankerite–siderite carbonatites (Fig. 5f). The ankerite–siderite carbonatite samples also have slightly higher Cl contents compared to other analysed biotite (Fig. 5d). Biotite from the Lyons River Sills, magnetite-biotite dykes, and silica-rich alkaline veins contain between 3 and 5 wt% F, although in some analyses from the silica-rich alkaline veins reach nearly 7 wt% F (Supplementary Material 2). These very high F contents exceed the supposed stoichiometric limit (~ 4.7 wt% F) but are similar to F-rich biotite reported by Petersen et al. (1982) and Motoyoshi and Hensen (2001).

Carbonate mineral chemistry

Dolomite from the Lyons River Sills contains 1.5–7.5 wt% FeO and 0.2–0.5 wt% MnO (Fig. 6a; Online Supplementary Material 3), 860 to > 3000 ppm Sr (Fig. 6a), and 9–122 ppm Zn. Calcite from the Lyons River Sills contains < 1 wt% FeO, less than < 1 wt% MnO, ~ 4500 ppm Sr (Fig. 6a), and ~ 1–2 ppm Zn (Fig. 6b; Supplementary Material 3). Siderite contains significant amounts of MnO (~ 6–17 wt%) and MgO (~ 9–14 wt %) and often < 1 wt% CaO. Siderite has lower Sr (2–44 ppm) and significantly

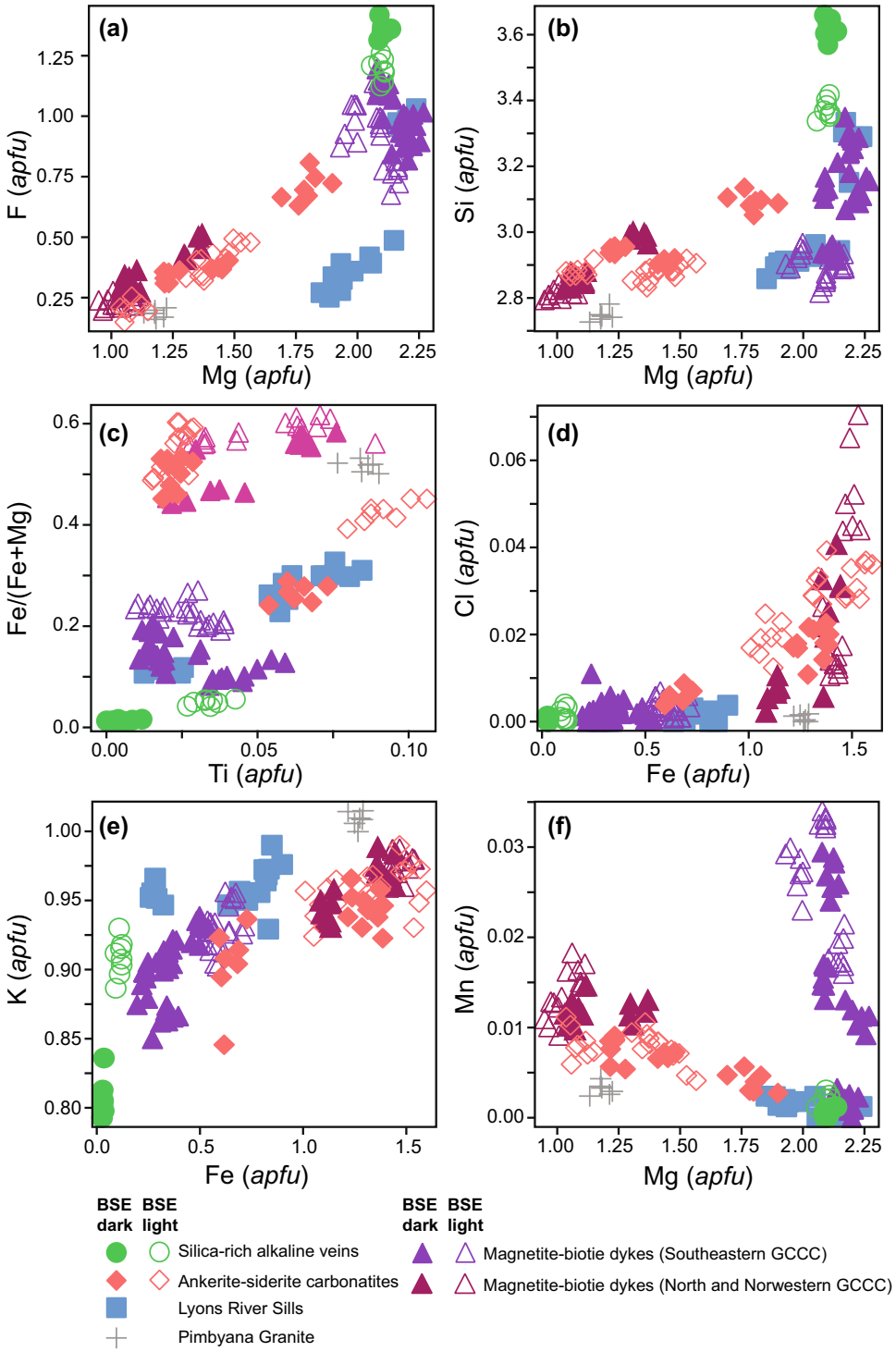

Fig. 5 Plots of biotite apfu and atomic Fe/(Fe + Mg). Closed symbols are dark zones and open symbols are light zones observed under BSE, respectively (see Fig. 4h for example image)

higher Zn contents (~ 260–12,000 ppm) compared to dolomite and calcite (Supplementary Material 3).

Chondrite-normalised REE + Y (REY) plots show that calcite is relatively LREE enriched, with a gentle, downward slope towards the HREE, but with a slight negative Y-anomaly (Fig. 6c). Dolomite has a flat trend across all REY and has a small negative Y-anomaly (Fig. 6c). Siderite is depleted in LREE and does not have a negative Y-anomaly but has HREE contents approaching that of dolomite and calcite.

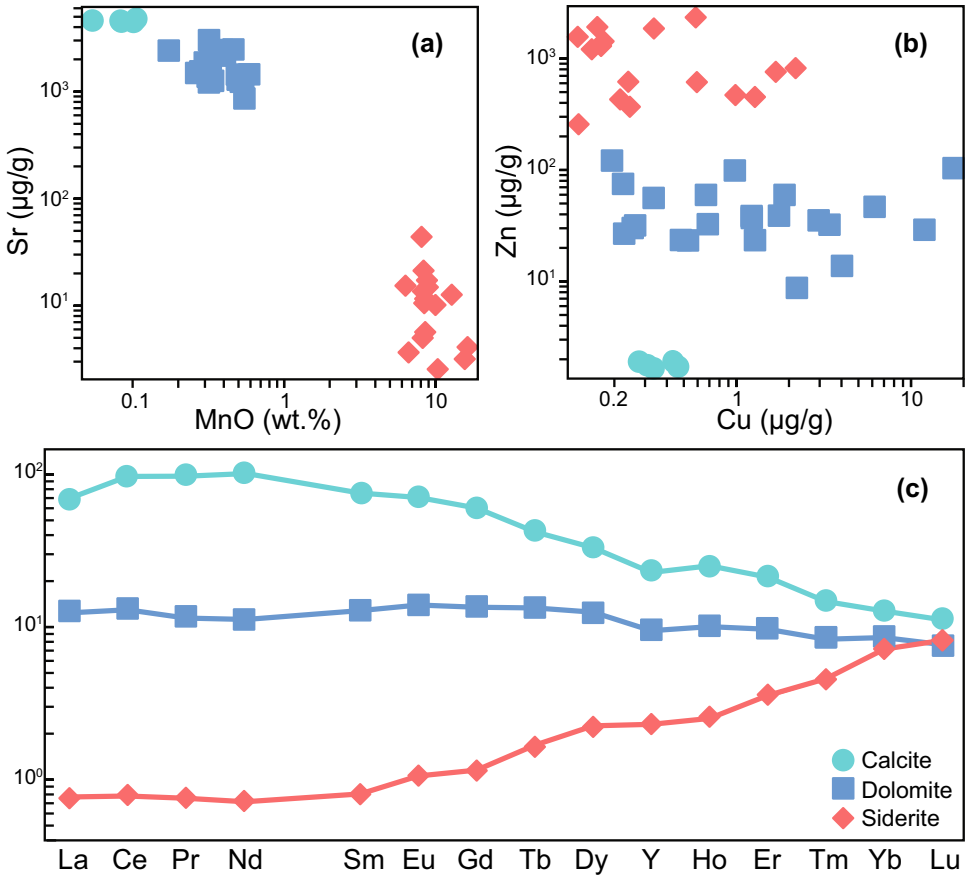

Fig. 6 Trace element plots for carbonate minerals. REY plots [normalised to values from McDonough and Sun (1995)] are averages of all analyses (Supplementary Material 3)

Whole rock chemistry

Lyons River Sills

Complete bulk rock geochemical data can be found in Supplementary Material 4. The Lyons River Sills are mainly classified as magnesiocarbonatites with only two samples falling within the calciocarbonatite range (Gittins and Harmer 1997; Fig. 7). Silica contents reach ~ 20 wt% SiO_2 for many of the dolomite-bearing samples (Fig. 8a), which also classifies them as silicocarbonatites according to Le Maitre (2002). The calcite carbonatites are rich in CaO and Sr, but contain relatively low TiO_2, MgO, Mg # (Mg/Mg + Fe), Ni, and Cr (Fig. 8b–d; Supplementary Material 4) compared to the dolomite carbonatites. The calcite carbonatites contain the highest phosphate contents. Apatite concentrated in layers was commonly observed in the calcite carbonatite samples, so the sampling of these layered zones may account for the high measured phosphate contents of some samples. In the dolomite carbonatites, CaO contents are antithetic with MgO, Fe_2O_3, and SiO_2 contents; and K_2O and Ti_2O contents increase with higher Fe_2O_3 contents (Fig. 8b, f). The green (aegirine > arfvedsonite) dolomite carbonatites

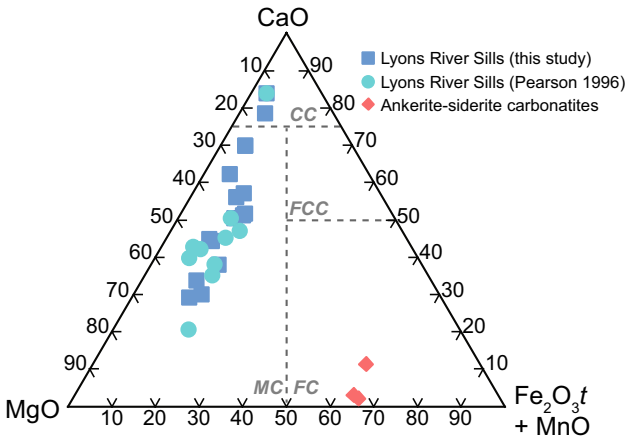

Fig. 7 Carbonatite classification plot using bulk rock molar CaO, MgO and Fe_2O_3 + MnO (after Gittins and Harmer 1997). Most of the Lyons River Sills from Pearson (1996) and this study fall within the magnesiocarbonatite field: three samples fall in the calciocarbonatite field. As the Lyons River Sills become more Mg-rich, their Fe content also increases. The ankerite–siderite carbonatites plot within the ferrocarbonatite field. *CC* calciocarbonatite, *FC* ferrocarbonatite, *FCC* ferruginous calciocarbonatite, *MC* Magnesiocarbonatite

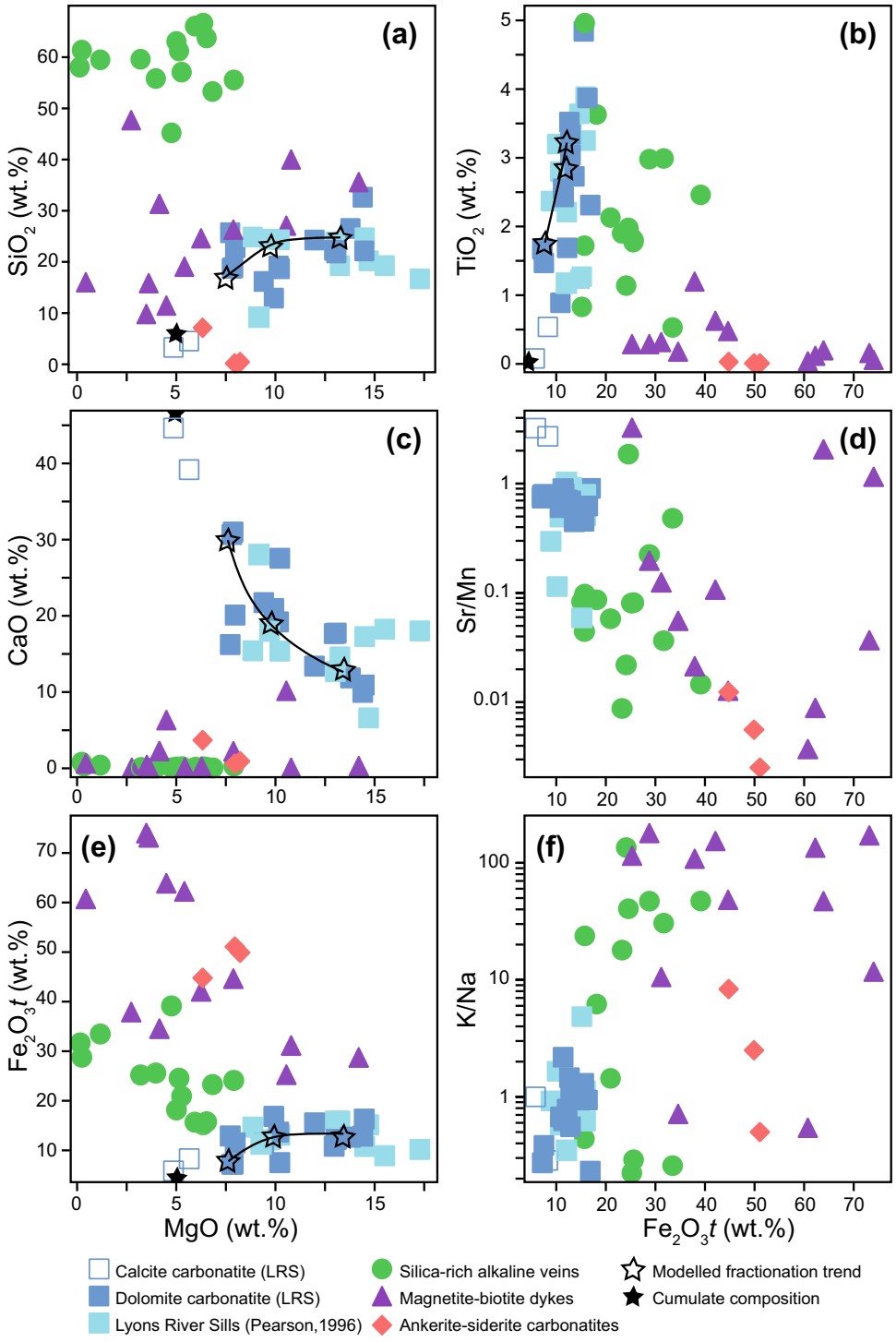

Fig. 8 Major element *X*–*Y* diagrams for various rock types of the GCCC. Iron contents are recast as total Fe_2O_3. Open black stars and black lines show calculated fractional crystallisation trends when a calcite-rich cumulate phase (solid black star) is separated from a dolomite carbonatite (see Table 3)

typically have higher Fe_2O_3 and Na_2O contents than their blue-coloured (aegirine < arfvedsonite) counterparts.

The calcite and dolomite carbonatites have similar trace element signatures, with both rock-types having high Ba, Th, and REY contents and dips in K, Pb, and Ti (Fig. 9a, b). The dolomite carbonatites also feature downward excursions in P. The fluorine contents in both rock types is variable, ranging between several hundred ppm up to ~ 9000 ppm.

Ankerite–siderite carbonatites

The ankerite–siderite carbonatites are Fe-rich and contain moderate MgO amounts and are comparable to the magnetite-biotite dykes in terms of total Fe_2O_3 and MgO contents (Fig. 8b, d, e). This carbonatite type also has the highest Mn contents and is enriched in Th and LREE, but has relatively low contents of SiO_2, CaO, Ba, Sr, HFSE (Nb, Ta, Zr, Hf,

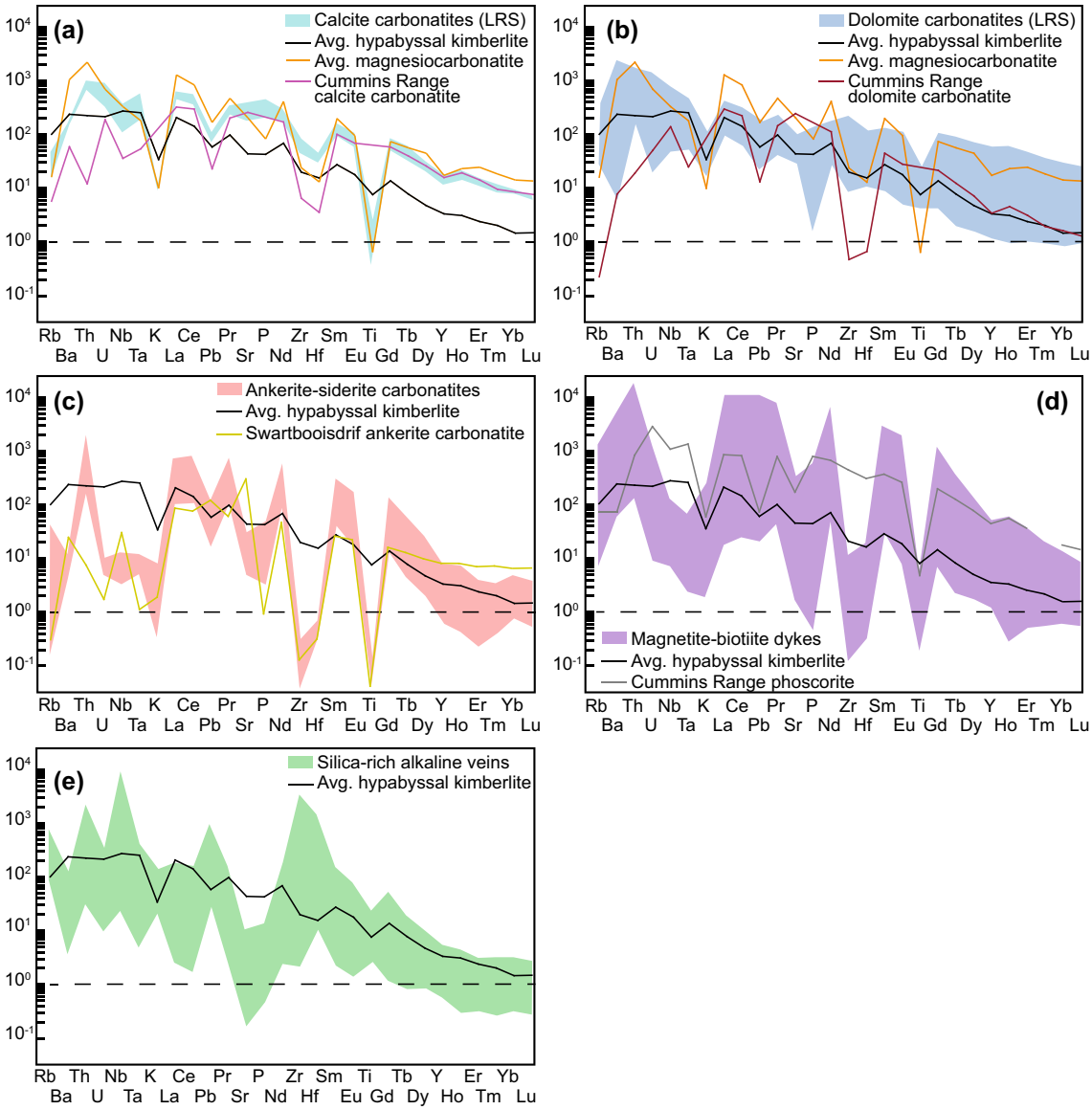

Fig. 9 **a**–**e** Trace element plots normalised to primitive mantle (Sun and McDonough 1989). The values for the average hypabyssal kimberlite and average magnesiocarbonatite are from Chakhmouradian et al. (2009). The values for the Cummins Range carbonatites and phoscorites (Australia) are from Downes et al. (2014). Tm is not shown in **d** because it is below the detection limit for Cummins Range phoscorites. Swartbooisdrif ankerite carbonatite (South Africa) data are from Thompson et al. (2002)

Ti), U, and, in some samples, HREE (Fig. 9c and Supplementary Material 6).

Magnetite-biotite dykes

The magnetite-biotite dykes have high Fe_2O_3 and K_2O and variable amounts of SiO_2 but have low TiO_2 and CaO contents compared to other rock types (Fig. 8). Most of the magnetite-biotite dykes contain more Mn than Sr, except for the three most Mg-rich samples (Fig. 8d).

Normalised trace element diagrams (Fig. 9d and Supplementary Material 6) show that the magnetite-biotite dykes are enriched in Th and LREE, with variable HREE contents. These rocks, together with the ironstones of the complex, contain most of the REE resources in the GCCC (Slezak 2019). The magnetite-biotite dykes also contain significant amounts of F (0.7–3.8 wt%) and Li (~ 1500 ppm; Supplementary Material 4), and have distinctly depleted Nb, Ta, Zr, Hf, and Ti contents.

Silica-rich alkaline veins

The silica-rich alkaline veins contain 45–67 wt% SiO_2, variable MgO, and relatively high TiO_2 contents (Fig. 8a,

b). Na_2O and K_2O contents range from 0.02 to 6.5 wt%, and 0.6 to 4 wt%, respectively, resulting in K/Na between ~ 1 and ~ 11 (Fig. 8f). The Sr/Mn ratios for these rocks fall between the Lyons River Sills and the magnetite–biotite dykes (Fig. 8d).

Trace element diagrams (Fig. 9e and Supplementary Material 6) show that the silica-rich alkaline veins have a positive Th anomaly, similar to the other rocks in the GCCC (Fig. 9e). They also have pronounced Nb enrichment, especially compared to Ta, and notable relative enrichment in Zr and Hf. Most of the silica-rich alkaline vein samples have low Sr, P, and HREE values (Fig. 9e). Lithium contents range from 16 ppm to greater than 2000 ppm, and F contents reach as high as 2.3 wt% (Supplementary Material 4).

Isotope data

Nd and Sr isotopes

Samarium–Nd isotope compositions were obtained for bulk rock samples representative of the different rock types including the Lyons River Sills, magnetite–biotite dykes, ankerite–siderite carbonatites, and silica-rich alkaline veins. A formation age of c. 1370 Ma was used to calculate initial εNd(t) values based on previous radiometric isotope dating of the GCCC (Zi et al. 2017; Slezak and Spandler 2019).

The εNd(t) values for the all rock-types of the GCCC range from − 1.8 to − 4 (Table 1). There is some minor regional variability, with samples near Yangibana North and West having slightly more negative values compared to the samples from the south and east of the Complex (Fig. 2). The T_{DM} ages generally range from c. 2100 to 1870 Ma (Table 1). The silica-rich alkaline veins samples returned εNd(t) values consistent with other results (εNd(t) = − 3.62 to − 3.90), but the Sm/Nd ratios were abnormally high, resulting in unreasonable T_{DM} ages. One Lyons River Sills sample and two silica-rich alkaline vein samples analysed by Pearson (1996) yielded εNd(t) values of − 1.57, and of − 0.55 and − 1.56, respectively (Table 1). These silica-rich alkaline vein samples contained lower $^{147}Sm/^{144}Nd$ ratios than the silica-rich alkaline vein samples measured in this study, and so returned similar T_{DM} ages to other rock-types of the GCCC (Table 1).

Strontium isotopes were obtained from the carbonate minerals separated from carbonatite samples (Table 2). Six dolomite carbonatite analyses resulted in $^{87}Sr/^{86}Sr$ ranging from 0.70570 to 0.71211 (Fig. 10). Three ankerite–siderite carbonatite samples contain higher ratios ranging from 0.71465 to 0.71996 (Table 2; Fig. 10).

Table 1 Bulk rock Nd isotope compositions

Sample	Rock type	Age (Ma)	Nd (µg/g)	Sm (µg/g)	$^{147}Sm/^{144}Nd$	$^{143}Nd/^{144}Nd$	2σ	$^{143}Nd/^{144}Nd$ (t)	εNd (t)	T_{DM} (Ma)	T_{CHUR} (Ma)
YN49-58.5	Ankerite–siderite carbonatite	1370	1080	137	0.076451	0.511431	0.0000032	0.510743	− 2.45	1890	1530
YN50-48.6	Ankerite–siderite carbonatite	1370	49.0	6.96	0.085773	0.511433	0.0000039	0.510661	− 4.07	2030	1650
LRS-16	Dolomite carbonatite	1370	92.2	14.7	0.096173	0.511519	0.0000029	0.510654	− 4.20	2100	1700
P016852[a]	Dolomite carbonatite	1370	57.7	7.79	0.077603	0.511523	n/a	0.510788	− 1.57	1860	1480
LRS-119	Calcite carbonatite	1370	371	64.6	0.10519	0.511706	0.0000030	0.510759	− 2.14	2000	1550
YW61-7.7	Magnetite–biotite dyke	1370	2370	327	0.083367	0.511467	0.0000027	0.510717	− 2.97	1950	1570
MOS-135	Magnetite–biotite dyke	1370	121	16.1	0.080447	0.511499	0.0000029	0.510775	− 1.83	1870	1490
DMCY-138	Magnetite–biotite dyke	1370	801	105	0.079431	0.511485	0.0000022	0.510770	− 1.92	1870	1500
YS-104	Silica-rich alkaline vein	1370	19.5	7.29	0.22637	0.512722	0.0000023	0.510685	− 3.60	− 5610	431
YS-105	Silica-rich alkaline vein	1370	7.09	2.06	0.17573	0.512250	0.0000029	0.510668	− 3.92	3510	2820
P17133[a]	Silica-rich alkaline vein	1370	64.8	4.82	0.064086	0.511245	n/a	0.510841	− 0.55	1710	1400
P17130[a]	Silica-rich alkaline vein	1370	239	50.7	0.058555	0.511943	n/a	0.510789	− 1.56	2130	1550

Age is time of emplacement from Slezak and Spandler (2019)

[a]Bulk rock Sm–Nd data from Pearson (1996) recalculated to t = 1370 Ma

Table 2 Sr, C, and O isotope data for carbonate minerals from the Lyons River Sills and ankerite–siderite carbonatites. $t = 1370$ Ma

Identifier	Rock type	Mineral (C–O isotopes)	$\delta^{13}C$‰VPDB	$\delta^{18}O$ ‰VSMOW	Sr (µg/g)	$^{87}Sr/^{86}Sr$	2σ	$\varepsilon Sr(t)$
LRS-1	Dolomite carbonatite	Dolomite	− 4.9	19.4				
LRS-16	Dolomite carbonatite	Dolomite	− 5.4	10.3				
LRS-117	Dolomite carbonatite	Dolomite	− 5.0	10.8				
LRS-119B	Calcite carbonatite	Calcite	− 5.6	9.2				
LRS-121	Calcite carbonatite	Calcite	− 5.4	10.1				
LRS-125	Dolomite carbonatite	Dolomite	− 4.4	26.6				
LRS-140	Dolomite carbonatite	Dolomite	− 5.3	10.5				
LRS-149A	Dolomite carbonatite	Dolomite	− 5.4	10.5	1370	0.70569	0.000010	− 9.08
LRS-149B	Dolomite carbonatite	Dolomite	− 5.4	10.2	1370	0.71209	0.000010	81.6
LRS-151	Dolomite carbonatite	Dolomite	− 5.1	10.6	1840	0.70686	0.000011	7.46
LRS-15A	Dolomite carbonatite	Dolomite	− 5.1	10.6	1520	0.70644	0.000012	1.58
LRS-15B	Dolomite carbonatite	Dolomite	− 5.1	10.2	1520	0.70656	0.000010	3.22
LRS-23	Dolomite carbonatite	Dolomite	− 5.7	10.7	2040	0.71115	0.000010	68.2
YN49-58.5	Ankerite–siderite carbonatite	Siderite	− 7.1	10.8	12.9	0.71464	0.000010	118
YN49-61.6	Ankerite–siderite carbonatite	Siderite	− 6.4	11.1	7.57	0.71985	0.000043	191
YN50-48.6	Ankerite–siderite carbonatite	Siderite	− 6.1	10.4	17	0.71881	0.000016	177

Strontium contents are averages from LA–ICP–MS analyses (Supplementary Material 3)

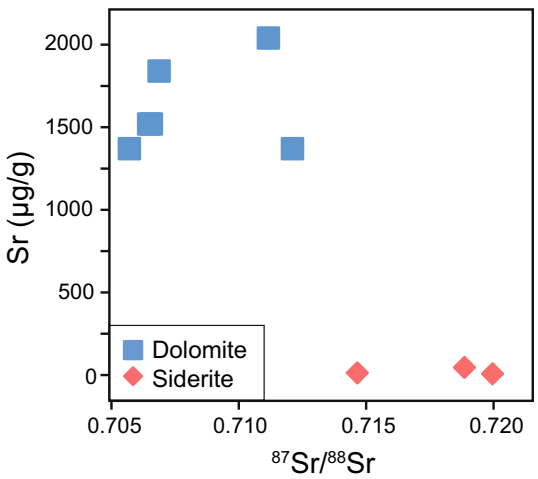

Fig. 10 Strontium contents and $^{86}Sr/^{87}Sr$ values for dolomite and siderite from the Lyons River Sills and ankerite–siderite carbonatites, respectively

C and O isotopes

The C and O isotope compositions of the various carbonatites are recognised to fall into three distinct populations (Fig. 11; Table 2). The $\delta^{18}O$ values for the main grouping of the dolomite carbonatites is between 10.2 and 10.8‰, while two calcite carbonatite samples yielded $\delta^{18}O$ values of 9.2‰ and 10.1‰. Both calcite and dolomite carbonatites have $\delta^{13}C$ values between − 5.0 and − 5.7‰. Two dolomite carbonatite analyses yielded $\delta^{18}O$ values of 19.4‰ and 26.6‰ and $\delta^{13}C$ values of − 4.9‰ and − 4.4‰, respectively. The $\delta^{13}C$ values are consistent with mantle values as established by both Taylor (1967) and Keller and Hoefs (1995), but the $\delta^{18}O$ values fall outside of the $\delta^{18}O$ mantle fields (Fig. 11). The ankerite–siderite carbonatites have much more negative $\delta^{13}C$ values ranging from − 6.1‰ to − 7.1‰, but similar $\delta^{18}O$ values ranging from 10.2 to 11.1‰ (Fig. 11).

Discussion

Definition and evolution of the Lyons River Sills

The Lyons River Sills are best defined as carbonatites based on their carbonate mineral composition (i.e., > 50 modal %; Le Maitre 2002). Because of their high Si content (~ 20 wt% SiO_2) and similar trace element characteristics, the Lyons River Sills were originally compared to carbonate-rich samples from the Benfontein kimberlites in South Africa (Pearson and Taylor 1996). Later, the Lyons River Sills were dubbed the Gifford Creek Ferrocarbonatite Complex by Pirajno et al. (2014) due to the high bulk Fe contents, which is actually an artifact of the significant magnetite content of these rocks. Trace element analyses confirm that the Lyons River Sills are enriched in incompatible elements (Fig. 9), Ni, and some samples contain significant TiO_2 contents (present as ilmenite); all of which can be considered characteristic of kimberlites and carbonate-rich kimberlites (Dawson and Hawthorne 1973; Le Maitre 2002 and references therein; Zurevinski and Mitchell 2011). Ga/Al ratios

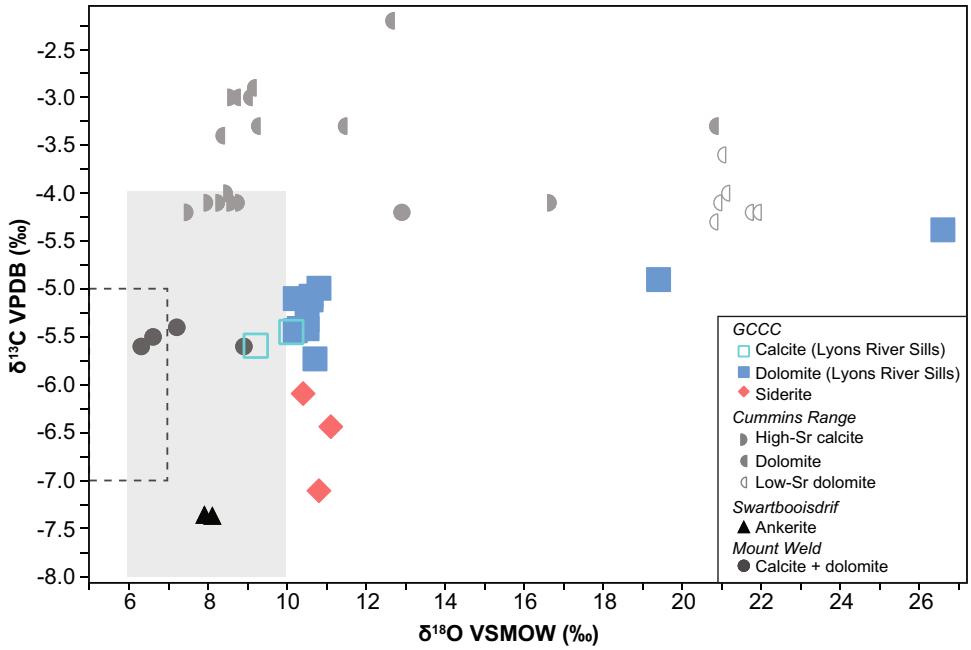

Fig. 11 Carbon-Oxygen isotope plots for the Lyons River Sills and ankerite–siderite carbonatites. The grey-shaded box is the mantle C–O isotope field from Taylor (1967) and the smaller, dashed box is the mantle C–O isotope field from Keller and Hoefs (1995)

of the Lyon River Sills (Fig. 12), together with the relatively low Na and high K contents of biotite from all rocks in the GCCC also correspond more closely to kimberlites than carbonatites (Chakhmouradian et al. 2009; Reguir et al. 2009). However, other features diagnostic of kimberlites, such as elevated Cr contents, the presence of perovskite, Mg- and Cr-rich ilmenite (Mitchell 1979), olivine, and mantle xenoliths were not observed in the GCCC. Furthermore, the Lyons River Sills have REY contents comparable to average magnesiocarbonatite, which are nearly an order of magnitude higher than an average hypabyssal kimberlite (Supplementary Material 6; Chakhmouradian et al. 2009). Here, the GCCC is also compared to the Cummins Range carbonatite complex (Halls Creek Orogen, Western Australia) due to its relative proximity to the GCCC and mid-Proterozoic age (Downes et al. 2014). The trace element composition of the Lyons River Sills and Cummins Range dolomite and calcite carbonatites are similar (Fig. 9a, b; Downes et al. 2014), although, the Cummins Range carbonatites have lower Ba, Hf, Rb, and Zr contents (Fig. 9a, b), which further attests to the ambiguous nature of the Lyons River Sills.

Origins for the Lyons River Sills can be further assessed using radiogenic and stable isotope data. The $\delta^{13}C$ and $\delta^{18}O$ values (Fig. 11) for the Lyons River Sills are broadly consistent with a mantle source, albeit with slightly elevated $\delta^{18}O$ values. The dolomite samples with excursions to $\delta^{18}O = 19.4‰$ and 26.6‰ could indicate contamination of sedimentary carbonates or fractionation within the units (Veizer et al. 1999; Demény et al. 2004). However, there is no evidence to suggest incorporation of sedimentary units nor is there a consistent fractionation trend. Our preferred interpretation is that the elevated $\delta^{18}O$ of these samples is due to post-magmatic, low temperature alteration of carbonate minerals, as discussed in more detail below.

The Lyons River Sills have similar Sr isotope compositions to the Phalaborwa carbonatite (Fig. 13; Eriksson 1989; Yuhara et al. 2005) and Group II kimberlites (Smith 1983), but slightly more radiogenic Nd isotope values. Collectively, the data are consistent with an enriched mantle source that is somewhat comparably to an idealised EM2-type source (Hart et al. 1992; Stracke et al. 2005; Stracke 2012) for the Lyons River Sills.

There is significant compositional variation in the Lyons River Sills (Figs. 7, 8), despite the fact that they occur congruently as an intrusive swarm subparallel to the Lyons River Fault (Fig. 2). Several different mechanisms can account for geochemical variability in carbonatite melts, including wall rock assimilation, reaction with the wall rock, fractional crystallisation, and liquid immiscibility. Wall rock assimilation and reaction are considered negligible in the Lyons River Sills, as wall rock xenoliths were not observed, and the thin carbonatite dykes/sills would have had a low thermal capacity in which to assimilate the wall rock. In addition, the C and radiogenic isotope compositions are consistent with an enriched mantle source (Figs. 11, 13), with limited to no crustal input.

The stability field of calcite in mantle-derived (Mg-rich) carbonatite increases with decreasing pressure (i.e., as the melt ascends), and in many cases, calcite is considered to be the liquidus phase (Harmer and Gittins 1997). The low viscosity of carbonatite melt (Kono et al. 2014) would facilitate separation of early-formed calcite (and other crystallised minerals) from liquid. In this scenario, the Lyons River Sills calcite carbonatites could represent crystal cumulates

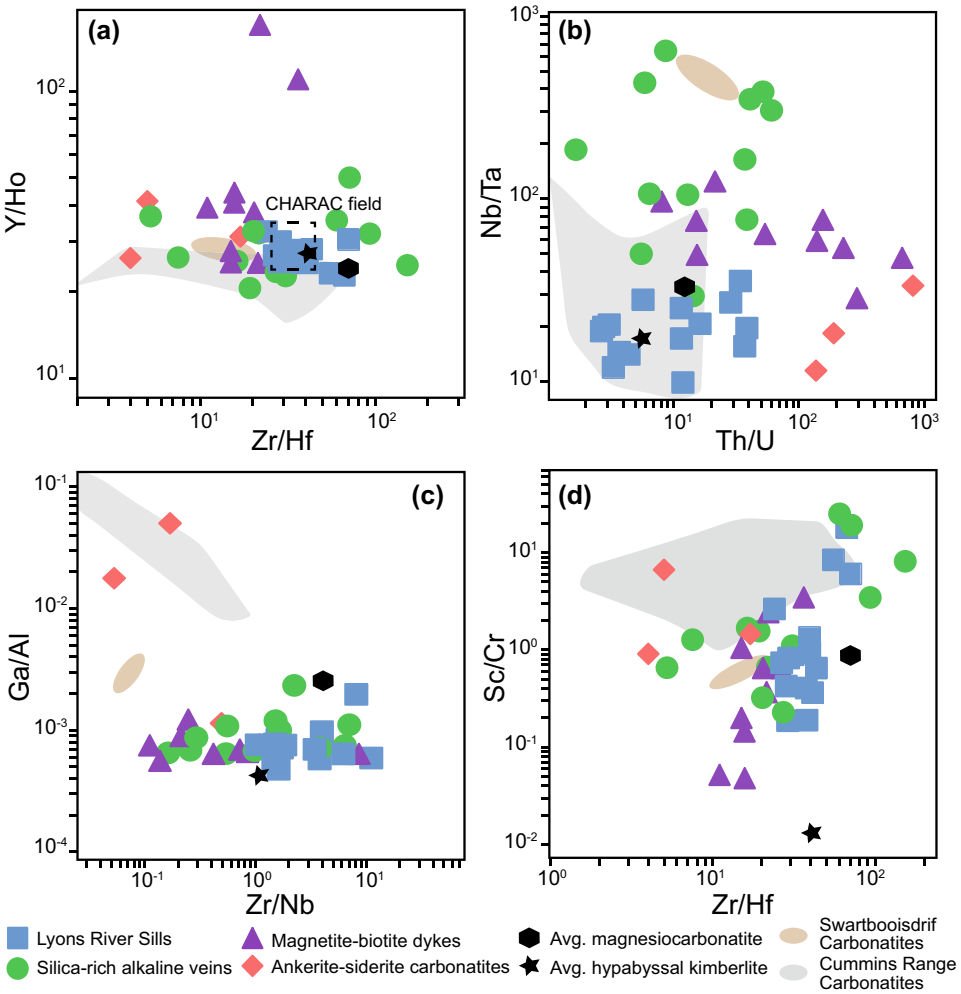

Fig. 12 Trace element ratios plotted for the different rock types in the GCCC. The values for the average hypabyssal kimberlite and average magnesiocarbonatite are from Chakhmouradian et al. (2009). The values for the Cummins Range carbonatites and phoscorites (Australia) are from Downes et al. (2014). Swartbooisdrif ankerite carbonatite (South Africa) data are from Thompson et al. (2002). The charge-and-radius-controlled (CHARAC) field is from Bau (1996)

(Harmer and Gittins 1997), and the melt would evolve towards more Fe- and Mg-rich values with progressive calcite-dominated fractionational crystallisation.

We undertook fractionation modeling to test whether the compositional variation observed in the Lyons River Sills could be explained by fractional crystallisation. The modeling was guided by mineral phases and proportions in the Lyons River Sills suite and involved progressive removal of various mineral components from melt compositions with a starting melt composition of a dolomite carbonatite with relatively high CaO and low MgO, TiO_2, and Fe_2O_3 contents (Table 3; Fig. 8). The first phase of fractionation involved crystallisation of calcite, dolomite, Mg-rich arfvedsonite, and apatite from the starting melt in quantities of 29%, 5%, 4%, and 1%, respectively (Table 3). These modelled fractionated components represent an early cumulate phase similar in composition to the calcite carbonatite samples (Fig. 8), particularly with respect to SiO_2, MgO, CaO, and Fe_2O_3, and TiO_2 contents. The P_2O_5 contents are low in the modelled cumulate phase compared to the actual calcite carbonatite samples, which is likely a result of sampling bias as apatite forms distinct layers within the calcite carbonatites. After removal of the cumulate phase, additional calcite and other mineral phases such as phlogopite were further removed from the residual melt (Residual melt 1 in Table 3), which resulted in the residual melts become enriched in MgO, Fe_2O_3, SiO_2, Na_2O, K_2O, Ti_2O, and Al_2O_3 (i.e., Residual melt 2 in Table 3); an evolutionary trend that compares closely to the compositional trends observed in the natural samples of dolomite carbonatites (Fig. 8; Table 3).

Because the increasing trends in MgO, Fe_2O_3, and TiO_2 are primarily driven by a loss of CaO as calcite, the calcite carbonatites in the Lyons River Sills likely represent an early cumulate phase. The separation of calcite and apatite as cumulus phases accounts for the substantial changes in P_2O_5 between carbonatite types. Biggar (1969) demonstrated that apatite and calcite can crystallise early in carbonatites creating flow banding, which is consistent with the apatite banding in the Lyons River Sill calcite carbonatites, as well as reports of apatite banding in East African carbonatites (Le Bas 1989 and references therein), and reports of cumulus calcite in the Kovdor

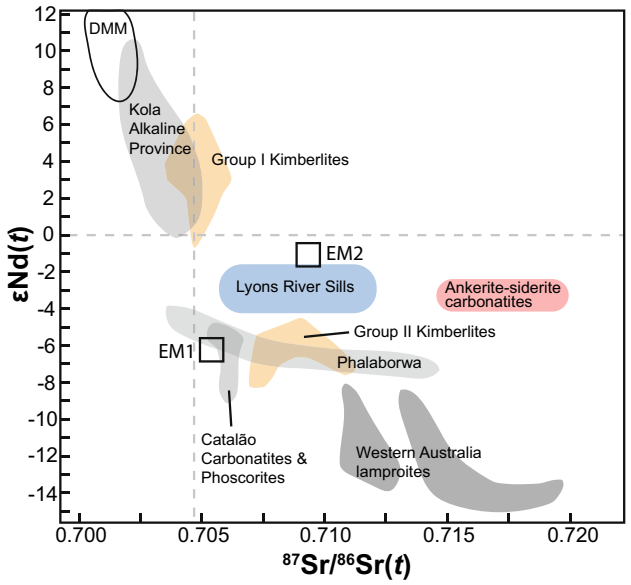

Fig. 13 Neodymium vs. Sr isotope plot for GCCC carbonatites and other alkaline magmatic rocks. The Lyons River Sills dolomite and calcite carbonatites plot between EM1 and EM2 with Sr isotope values overlapping with EM2. The ankerite–siderite carbonatites have highly radiogenic Sr isotope values. Data for other complexes include: Kola Alkaline Province, Russia (Zaitsev and Bell 1995; Dunworth and Bell 2001); Catalão carbonatites and phoscorites, Brazil (Cordeiro et al. 2010); Phalaborwa, South Africa (Eriksson 1989; Yuhara et al. 2005); WA lamproites (Nelson et al. 1986); DMM, EM1, EM2 (Hart et al. 1992; Stracke et al. 2005; Stracke 2012), and; Group I and II kimberlites (Smith 1983)

ultramafic alkaline Complex (Harmer and Gittins 1997; Veksler et al. 1998). Removal of CaO (mainly in calcite) from the carbonatite melt and residual liquid evolution to higher MgO and Fe_2O_3 contents has been modelled and observed in other carbonatite systems (Wyllie 1965; Woolley and Kempe 1989). The trend from Mg-rich to Fe-rich compositions is also consistent with the Fe/Mg content of biotite (Supplementary Material 5 and Fig. 5) from these rocks. Calcite dominated fractionation is also consistent with an increase in MnO and decrease in Sr contents in the melt, which is also reflected in the dolomite compositions (Fig. 8).

Although the modeling predicts that melt Na_2O and K_2O contents should increase during fractionation, the concentration of these elements is variable in the natural samples. The sampled carbonatites likely do not represent pristine melt compositions (Woolley and Church 2005), and alkali elements are likely to remain incompatible during fractionation (as is consistent with extensive fenitisation of the wall rocks outside of the carbonatites). The small size and patchy, pervasive nature of aegirine throughout the Lyons River Sills indicates that aegirine is likely a later alteration phase, potentially related to alkali (e.g., K ↔ Na) exchange with the granite wall rock via fenitising fluids.

Origin of the ankerite–siderite carbonatites

Ferrocarbonatites are an uncommon carbonatite type and are generally considered to be the last phase to form in a carbonatite fractionation sequence (Le Bas 1977, 1989; Zaitsev et al. 2004). Many ferrocarbonatites—especially those dominated by siderite—are reported to be of hydrothermal origin, occurring at temperatures as low as 150 °C (Simonetti and Bell 1994; Zaitsev et al. 2004). Nonetheless, there are several documented cases of magmatic ferrocarbonatites including the Newania carbonatites in India (Woolley and Buckley 1993), the Swartbooisdrif ferrocarbonatites of Namibia (Thompson et al. 2002), and the ferrocarbonatites of Central Tuva, Russia (Prokopyev et al. 2016). These carbonatite complexes are interpreted to have formed at temperatures between ~ 420 and 850 °C (Drüppel et al. 2004; Prokopyev et al. 2016).

The ankerite–siderite carbonatites of the GCCC are similar to the Swartbooisdrif ferrocarbonatites as both show depletion in Hf, Rb, Ti, and Zr; have low Cu contents; display enrichment in the LREE; have overlapping Zr/Hf, Zr/Nb, and Y/Ho values (Figs. 9c, 12); and have similar $\delta^{13}C$ values (Fig. 11). However, the ankerite–siderite carbonatites have an order of magnitude greater Zn contents and higher $\delta^{18}O$ values (10–11‰ versus ~ 8‰; Fig. 11) than the Swartbooisdrif ferrocarbonatites. Fluorine and estimated OH contents for biotite (Supplementary Material 2) and apatite (Slezak et al. 2018) were applied to the F-OH biotite-apatite thermometric relations of Sallet (2000) to calculate an approximate temperature range of ~ 600–700 °C for the ankerite–siderite carbonatites. These results are in line other ferrocarbonatite temperature ranges and fall within the siderite stability field at ~ 1 GPa (Tao et al. 2013).

Carbonate minerals from the ankerite–siderite carbonatites have similar $\delta^{18}O$ values, but distinctly lower $\delta^{13}C$ values (Fig. 11) and highly radiogenic $^{86}Sr/^{87}Sr$ values (average $^{86}Sr/^{87}Sr = 0.7175$; Table 2) when compared to the Lyons River Sills carbonates (Figs. 10, 13). The elevated Sr isotope composition of the ankerite–siderite carbonatites is particularly striking, as it is not associated with a comparable unradiogenic Nd isotope composition (Fig. 13), and hence is not attributed to any putative mantle source, or to variable degrees of assimilation of the continental-type local host rocks. Previous work has demonstrated that rocks of the complex have experienced widespread recrystallisation and isotopic resetting due to tectonism and hydrothermal alteration that postdates magmatic emplacement by up to ~ 500 m.y. (Zi et al. 2017; Slezak et al. 2018; Slezak and Spandler 2019). Therefore, we propose that the elevated Sr isotope values reflect post-magmatic carbonate recystallisation (via metamorphic or hydrothermal alteration) of the carbonate minerals, allowing incorporation of highly radiogenic Sr from the local crustal rocks. The ankerite–siderite

Table 3 Fractional crystallisation modelling of the Lyons River Sills carbonatite magma evolution

	Starting composition	Cumulate phase	Residual melt 1	Residual melt 2
SiO_2	16.0	6.17	22.4	24.6
Al_2O_3	0.78	0	1.27	1.00
FeO	7.22	1.02	11.2	11.2
MgO	7.55	5.00	9.29	13.0
CaO	29.8	49.0	18.8	12.8
Na_2O	1.26	1.20	1.33	1.63
K_2O	1.26	0	2.06	1.94
TiO_2	1.72	0	2.82	3.22
P_2O_5	0.43	1.12	0.01	0.01
MnO	0.73	0	1.19	1.4
CO_2	33.2	36.5	29.6	29.2
Total	100	100	100	100
Mineral phase		% Removed		% Removed
Calcite		29		40
Dolomite		5		
Mg-arfvedsonite		4		
Arfvedsonite				4
Phlogopite				2
Apatite		1		1
Total		39		47

The modelled cumulate phase is similar to the calcite carbonatite sample LRS-119. Residual melts 1 and 2 are comparable to the dolomite carbonatite samples LRS-149 and LRS-118, respectively (Supplementary Material 4)

carbonatites contain an order of magnitude less Sr than the Lyons River Sills carbonates (Fig. 10), so incorporation of crustal Sr will have noticeably greater effect on the Sr isotope composition of the ankerite–siderite carbonatites, as observed. The relatively low $\delta^{13}C$ values (Fig. 11) are also consistent with late-stage recrystallisation, as low T CO_2 loss via fluid alteration will shift $\delta^{13}C$ values of Fe-carbonates to more negative values (Deines 2004).

Field observation of the relationship between the ankerite–siderite carbonatites and other primary rock types in the GCCC are lacking, so the genetic relationship with other units is enigmatic. Other magmatic ferrocarbonatites such as those from Swartbooisdrif (Namibia) and Central Tuva (Russia) occur in alkaline provinces as the predominant carbonatite type (Thompson et al. 2002; Drüppel et al. 2004; Propkoyev et al. 2016) whereas in the GCCC, the ankerite–siderite carbonatites are subordinate to the calcite and dolomite carbonatites of the Lyons River Sills. Woolley (1982) and Le Bas (1989) demonstrated that ferrocarbonatites could be created through multiple fractionation paths beginning with calcite carbonatites. However, fractionation modelling from the Lyons River Sills to the ankerite–siderite carbonatites could not reproduce the low Si and Ti contents of the ankerite–siderite carbonatites. The ankerite–siderite carbonatites may be related to the Lyons River Sills by an unidentified intermediate phase at depth, or the different carbonatites may relate to separate, as yet unrecognised, primary magmas generate by melting of heterogeneities in the mantle source (Bell et al. 1982; Yaxley et al. 2019).

Magnetite–biotite dykes: connections to carbonatites

Globally, phoscorites are uncommon rocks that are spatially associated with carbonatites (Woolley and Kjarsgaard 2008), but their genetic relationships are ambiguous. Phoscorites were originally defined as having a magnetite + apatite + forsterite assemblage (Russel et al. 1954), but now the definition includes diopside and phlogopite as additional silicate phases (Krasnova et al. 2004). Glimmerites can also be spatially associated with carbonatites, but these are distinguished from phoscorites by their biotite-dominant mineralogy (Le Maitre 2002), and are now considered to be of metasomatic origin (Elliott et al. 2018).

Despite our previous classification (see Slezak et al. 2018 and Slezak and Spandler 2019), the magnetite-biotite dykes of the GCCC are not phoscorites sensu stricto as they lack diopside or forsterite and often have more monazite that apatite. Nevertheless, these rock-types are similar enough to warrant comparisons. Compared to the phoscorites in the Cummins Range, Australia (Downes et al. 2014), the magnetite–biotite dykes in the GCCC have lower Hf, Nb, Ta,

and Zr contents and higher Th and LREE contents (Figs. 9d and Supplementary Material 6). Both the Cummins Range phoscorites and the GCCC magnetite-biotite dykes have negative Ti anomalies and comparable Ba and Pb contents (Fig. 9d). The high monazite content relative to apatite of the magnetite biotite dykes may reflect the high bulk REE contents relative to Ca.

Magnetite–biotite dyke are found in two localities in the GCCC: (1) southeast, and (2) northern/northwest (Fig. 2). The magnetite–biotite dykes in the southeast region contain higher Mg, Ni, and Cr, and lower Fe compared to those of the northwest region. The southeastern magnetite–biotite dykes also contain early apatite with REY patterns enriched in La and Ce, with later apatite zones having REY patterns enriched in Nd and Sm. The north and northwestern magnetite–biotite dykes contain MREE–enriched apatite, which is similar to the apatite from the ankerite–siderite carbonatites (Slezak et al. 2018). Biotite from the north and northeastern magnetite–biotite dykes contains higher Fe, Al, and Cl contents than those dykes in the southeastern region (Supplementary Material 5; Fig. 5). The biotite from these north and northeastern dykes is similar to the biotite from the ankerite–siderite carbonatites. The magnetite–biotite dykes and ankerite–siderite carbonatites also share similar bulk rock Fe_2O_3 and MgO compositions, have low Sr/Mn ratios (Fig. 8d, e), and display similar trace element features (i.e., relative enrichment in Th and REE, and relative depletion in Nb, Ta, Zr, Hf, and Sr; Fig. 9c, d). These spatial and geochemical similarities suggest that the magnetite-biotite dykes and ankerite–siderite carbonatites may be genetically related. Models involving fractionation and/or liquid immiscibility have been proposed to explain occurrences of coeval carbonatite and phoscorite elsewhere (Vartiainen 1980; Kogarko et al. 1997; Krasnova et al. 2004). Nonetheless, there has been relatively little research on the relationships between these two rock types, and direct field relations between the ankerite–siderite carbonatites and magnetite-biotite dykes of the GCCC are lacking. Therefore, the genetic links between these rock units cannot be evaluated any further at present.

Origin of the silica-rich alkaline veins

The silica-rich alkaline veins have a wide range in K/Na ratios that can broadly be grouped into of a high K group (K/Na > 1) and a high Na group (with K/Na < 1) (Fig. 8f). The difference in K/Na is related to alteration, with variable alteration of primary phlogopite resulting in K loss. The silica-rich alkaline veins with higher K contents often contain more phlogopite and higher Rb/Sr values. The high Na silica-rich alkaline veins contain fine-grained aegirine and are more strongly altered and sheared. Both units contain elevated levels of Si and Nb (as columbite and Nb-bearing rutile) and accommodate significant amounts of Zr (as zircon) and Ti (as rutile), suggesting that these rocks are altered variants of the same unit.

The normalised trace element plots of the silica-rich alkaline veins appear to be antithetic to those of the magnetite-biotite dykes and ankerite–siderite carbonatites (Fig. 9c–e). Where the magnetite–biotite dykes (and ankerite–siderite carbonatites) are depleted Nb, Zr, Hf, and Ti and enriched in Ba and REE, the silica-rich alkaline veins are relatively enriched in Nb, Zr, Hf, and Ti and depleted in Ba and REE. This geochemical association, together with the observation of thin silica-rich alkaline veins mantling a magnetite-biotite dyke at the Demarcay prospect (Fig. 3d), suggests that the silica-rich alkaline veins represent products of a magmatic-hydrothermal fluid phase released from the magnetite-biotite dykes. After the crystallisation of the magnetite-biotite dykes, this incompatible HFSE- and Fe-rich fluid phase migrated into fractures and joints. Secondary alteration and replacement of phlogopite by aegirine may be related to reaction of the veins by fenitising fluids from the host rocks.

Though often considered immobile in fluids, HFSE elements can be highly concentrated in peralkaline melts (Nicholls and Carmichael 1969; Watson 1979), and can be remobilised in Na- and F-rich hydrothermal fluids (Rubin et al. 1993; Salvi and Williams-Jones 1996; Jiang et al. 2005). Zirconium and Ti mobility is enhanced by F complexes such as ZrF_6^{2-} and TiF_6^{2-} (Barsukova et al. 1979; Salvi and Williams-Jones 1996; Jiang et al. 2005), and Nb is mobile in fluids under conditions of high F activity where it occurs as niobium hydroxyl-fluoride species (Timofeev et al. 2015). The HFSE likely became increasingly incompatible as the magnetite- and biotite-rich melts crystallised, and subsequently were partitioned with F-rich magmatic-hydrothermal fluids exsolved from these melts. These F-rich fluids then incorporated and reacted with the local host rocks (e.g., Pimbyana Granite) causing a decrease in temperature and an increase in Si activity which promoted zircon stability and precipitation of zircon in the veins (Salvi and Williams-Jones 1996; Chakhmouradian and Williams 2004; Gervasoni et al. 2017). Progressive wall rock reaction and precipitation of F-bearing phlogopite may have decreased the F activity in the fluid, allowing other HFSE-bearing minerals to precipitate (Timofeev et al. 2015).

Origins of the GCCC

The GCCC contains a wide array of alkaline rock types that occur together spatially but lack distinct field relationships with each other. Age data from Zi et al. (2017) and Slezak and Spandler (2019), puts emplacement of all the units in the GCCC at c. 1370 Ma, although there is substantial evidence for post emplacement recrystallisation of

the REE minerals (see Slezak and Spandler 2019). Bulk rock εNd (t=1370 Ma) values range from − 1.83 to − 4.20, which, together with the C, O, and Sr isotope composition of the Lyons River Sills, is consistent with an enriched mantle source for these rocks (Hart et al. 1992; Stracke et al. 2005; Stracke 2012). The relatively high Ti contents of the GCCC—and the Cummins Range carbonatite complex of the nearby Halls Creek Orogen—(Fig. 9b), are also consistent with derivation from an enriched mantle source such as EM2 modelled by Workman et al. (2004).

Mantle plume activity has been linked to c. 1380 Ma magmatism in central Africa and North America (Ernst 2014), but these areas were very distant (i.e., 1000 s of kms) from the GCCC at this time (Pisarevsky et al. 2014). There is no evidence to indicate any mantle plumes activity in the region at 1370 Ma so the GCCC is not considered to be linked with hotspot magmatism (Zi et al. 2017; Slezak and Spandler 2019). Calculated model T_{DM} ages from bulk-rock Nd samples are between c. 2100 and 1900 Ma, which is consistent with timing of convergence and collision of the Yilgarn Craton with the Glenburgh Terrane during the 2005–1950 Ma Glenburgh Orogeny (Occhipinti et al. 2004; Johnson et al. 2011). Plate convergence and subduction of hydrated ocean crust beneath the Glenburgh Terrane likely led to subduction-induced metasomatism of the mantle lithosphere (Fig. 14; Pilet et al. 2005). This metasomatised mantle is regarded to be the source of the carbonatitic parental magmas of the GCCC at c. 1370 Ma (Fig. 14). The precise mechanism responsible for mantle melting is unknown, but may relate to displacement of the lithospheric-scale Lyons River Fault, allowing low degree melting of the lithospheric mantle to produce primary alkaline magmas (Fig. 14). The Lyons River Fault likely acted as a conduit for these magmas to traverse the lithosphere to be emplaced in the upper crust. Such hypabyssal carbonatite complexes consisting of dykes/sills are typically emplaced in extension-related stress fields that allow for passive emplacement as tabular bodies instead of volcanic breccias or plutonic plugs (Barker 1989). Therefore, more broadly, carbonatite magmatism in the GCCC may have been related to far-field stresses associated with the separation of the North China Craton from the West Australia Craton during Nuna disassembly (Pisarevsky et al. 2014; Slezak and Spandler 2019). This model for the GCCC conforms to the general model for carbonatite formation of Woolley and Bailey (2012) and genetic models for many other REE ore deposits (e.g., Downes et al. 2014; Huston et al. 2016).

General implications for carbonatite magmatism

Studying the diversity of alkaline magmatic and hydrothermal rocks of the GCCC provides insights into other records of intraplate alkaline magmatic processes more broadly. Though the various units of the GCCC have stable and radiogenic compositions that point to a common enriched mantle source, there is significant geochemical heterogeneity among these rock types. Chemical heterogeneity within the Lyons River Sills can be attributed to fractionational crystallisation and cumulate processes that occurred within the metre- to sub-metre scale dykes/sills. Dykes and sills of this scale in silicate melts are widely regarded to preserve melt compositions as very little to no crystal accumulation is expected due to melt viscosity constraints. The operation of cumulate processes within such narrow carbonatite dykes/sills is likely due to the low viscosity of these melts (Kono et al. 2014) and indicates that even small carbonatites bodies

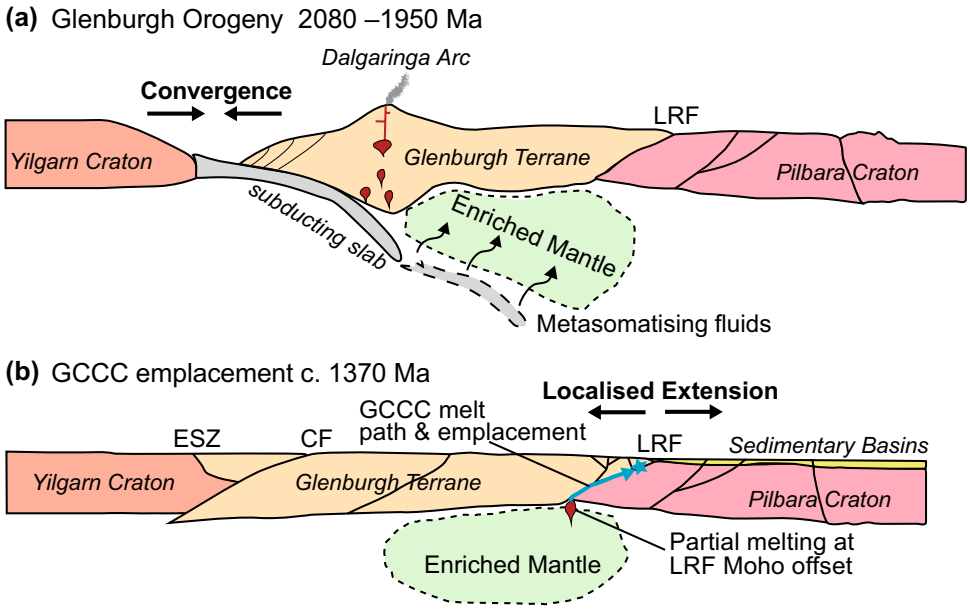

Fig. 14 **a** Mantle metasomatism under the Glenburgh Terrance resulting from plate subduction during the Glenburgh Orogeny (2018–1950 Ma). **b** Localised extension caused minor decompression melting at the Lyons River Fault Moho offset, creating the alkaline melts that travel along the fault and are emplaced as the GCCC. *CF* Cardilya Fault, *ESZ* Errabiddy Shear Zone, *LRF* Lyons River Fault. Modified from Johnson et al. (2011, 2013)

should not be assumed to reflect primary carbonatite magma compositions (see also Woolley and Church 2005).

Fractionation plays an important role in enriching carbonatites in Fe, Mn and LREE (Le Bas 1989) as well as enriching peralkaline melts in HFSE (Spandler and Morris 2016). The ankerite–siderite carbonatites and magnetite-biotite dykes likely represent more fractionated magmatic rock-types of the GCCC and both contain significant LREE resources (Slezak 2019). The occurrence of these Fe-rich rock-types could therefore be considered a key criterion for the REE ore potential of carbonatite complexes. Likewise, hydrothermal veins formed by fluids exsolved from crystallising carbonatite magma (such as the silica-rich alkaline veins of the GCCC) may be potential rare metal (Zr, Hf, Nb, Ta, etc.), resources, as these elements can be partitioned into alkaline fluids with high F contents.

Carbonatite complexes often have variable and highly radiogenic Sr isotope compositions that are interpreted prevailingly to reflect variably enriched mantle sources (Bell and Blenkinsop 1987). The highly radiogenic Sr isotope values of the GCCC ankerite–siderite dykes, especially compared with the Lyons Rivers Sill that have similar Nd isotopes compositions (Fig. 13), are an example of potential isotopic resetting through recrystallisation of carbonate minerals by post-magmatic hydrothermal/metamorphic events. Precambrian carbonatite complexes with complex post-emplacement histories and magmatic carbonates with low Sr contents (Fig. 10) are most susceptible to isotopic resetting, and we urge for caution in interpreting mantle source compositions from the Sr isotope composition of carbonatites in isolation of other geochemical and isotopic data.

Conclusions

1. The GCCC contains a range of rock types including calcite, dolomite, and ankerite–siderite carbonatites; magnetite-biotite dykes; and silica-rich alkaline veins. Alteration assemblages such as fenites and glimmerites are also present.
2. Compositional variation of the Lyons River Sills can be explained by fractional crystallisation and separation of an early calcite-bearing cumulate phase from the carbonatite melt, leading to Mg and Fe (+ Ti, Si, alkali) enrichment in the melt.
3. The ankerite–siderite carbonatites are interpreted to be of magmatic origin. The magnetite-biotite dykes and ankerite–siderite carbonatites have similar trace element contents, suggesting they are likely related, but the processes connecting them are still enigmatic. The relationship between these rock types and the Lyons River Sills remains uncertain.
4. The silica-rich alkaline veins are products of hydrothermal fluids enriched in Na, F, and HFSE that exsolved from the magnetite-biotite dykes and/or ankerite–siderite carbonatites during emplacement.
5. Parental magmas to the GCCC likely formed from melting of mantle lithosphere metasomatised during plate convergence and collision between the Yilgarn Craton and Glenburgh Terrane (c. 2000 Ma). Partial melting may have been triggered by reactivation of this suture zone due to far-field stresses associated with separation of the North China and West Australia Cratons at 1370 Ma.

Acknowledgements An ARC Future Fellowship (FT 120100198) to Carl Spandler supported this study. We thank Hasting Technology Metals Limited for their sample contributions and hospitality while conducting fieldwork. We also thank Jen Wan from the JCU AAC for her support with the C-O isotope analyses, Christa Placzek for her help with the Sr isotope analyses, as well as Kevin Blake and Shane Askew from the JCU AAC for their assistance with the EPMA analysis. We thank Sam Broom-Fendley, Francisco Pirajno, as well as the editor, Steven Reddy, for their reviews, which improved this manuscript.

References

Barker DS (1989) Field relations of carbonatites. In: Bell K (ed) Carbonatites: Genesis and Evolution. Unwin Hyman, London, pp 38–69

Barsukova ML, Kuznetsov VA, Dorofeyva VA, Khodakovskiy LI (1979) Measurement of the solubility of rutile TiO_2 in fluoride solutions at elevated temperatures. Geochem Int 7:41–49

Bau M (1996) Controls on the fractionation of isovalent trace elements in magmatic and aqueous systems: evidence from Y/Ho, Zr/Hf, and lanthanide tetrad effect. Contrib Miner Petrol 123:323–333

Bell K, Blenkinsop J (1987) Nd and Sr isotopic compositions of East African carbonatites: implications for mantle heterogeneity. Geology 15(2):99–102

Bell K, Blenkinsop J, Cole TJS, Menagh DP (1982) Evidence from Sr isotopes for long-lived heterogeneities in the upper mantle. Nature 298(5871):251–253

Biggar GM (1969) Phase relationships in the join $Ca(OH)_2$–$CaCO_3$–$Ca_3(PO_4)$–H_2O at 1000 bars. Miner Mag 37:75–82

Chakhmouradian AR, Williams CT (2004) Mineralogy of high-field-strength elements (Ti, Nb, Zr, Ta, Hf) in phoscoritic and carbonatitic rocks of the Kola Peninsula, Russia. In: Wall F, Zaitsev AN (eds) Phoscorites and carbonatites from mantle to mine: the key example of the kola alkaline province. The Mineralogical Society of Great Britain and Ireland, Cambridge, pp 293–340

Chakhmouradian AR, Böhm CO, Demény A, Reguir EP, Hegner E, Creaser RA, Halden NM, Yang P (2009) "Kimberlite" from Wekusko Lake, Manitoba: actually a diamond-indicator-bearing dolomite carbonatite. Lithos 112:347–357

Cordeiro PFO, Brod JA, Dantas EL, Barbosa ESR (2010) Mineral chemistry, isotope geochemistry and petrogenesis of niobium-rich rocks from the Catalão I carbonatite-phoscorite complex, Central Brazil. Lithos 118:223–237

Dawson JB, Hawthorne JB (1973) Magmatic sedimentation and carbonatitic differentiation in kimberlite sills at Benfontein, South Africa. J Geol Soc Lond 129:61–85

Deines P (2004) Carbon isotope effects in carbonate systems. Geochim Cosmochim Acta 68(12):2659–2679

Demény A, Sitnikova MA, Karchevsky PI (2004) Stable C and O isotope compositions of carbonatite complexes of the Kola Alkaline Province: phoscorite–carbonatite relationships and source compositions. In: Wall F, Zaitsev AN (eds) Phoscorites and carbonatites from mantle to mine: the key example of the kola alkaline province. Mineralogical Society of Great Britain & Ireland, London, pp 407–429

Downes PJ, Demeny A, Czuppon G, Jaques AL, Verall M, Sweetapple M, Adams D, McNaughton NJ, Gwalani LG, Griffin BJ (2014) Stable H–C–O isotope and trace element geochemistry of the Cummins Range Carbonatite Complex, Kimberley region, Western Australia: implications for hydrothermal REE mineralization, carbonatite evolution and mantle source regions. Miner Depos 49:905–932

Drüppel K, Hoefs J, Hoefs JMO (2004) Fenitizing processes induced by ferrocarbonatite magmatism at Swartbooisdrif, NW Namibia. J Pet 46(2):377–406

Dunworth EA, Bell K (2001) The Turiy Massif, Kola Peninsula, Russia: isotopic and geochemical evidence for multi-source evolution. J Pet 42:377–405

Elliott HAL, Wall F, Chakhmouradian AR, Siegfried PR, Dahlgren S, Weatherley S, Finch AA, Marks MAW, Deady E (2018) Fenites associated with carbonatite complexes: a review. Ore Geol Rev 98:38–59

Eriksson SC (1989) Phalaborwa: a saga of magmatism, metasomatism and miscibility. In: Bell K (ed) Carbonatites: genesis and evolution. Unwin Hyman, London, pp 221–254

Ernst RE (2014) Large igneous provinces. Cambridge University Press, Cambridge

Gellatly DC (1975) Yangibana Creek U-Th-REE-base metal prospect, Gascoyne Goldfield. Amax Exploration (Australia) Inc, W.A

Gervasoni F, Klemme S, Rohrbach A, Brutzner T, Berndt J (2017) Experimental constraints on the stability of baddeleyite and zircon in carbonate- and silicate-carbonate melts. Am Miner 102:860–866

Gittins J, Harmer RE (1997) What is ferrocarbonatite? A revised classification. J Afr Earth Sc 25(1):159–168

Harmer RE, Gittins J (1997) The origin of dolomitic carbonatites: field and experimental constraints. J Afr Earth Sc 25(1):5–28

Hart SR, Hauri EH, Oschmann LA, Whitehead JA (1992) Mantle plumes and entrainment: isotopic evidence. Science 256:517–520

Huston DL, Maas R, Cross A, Hussey KJ, Mernagh TP, Fraser G, Champion DC (2016) The Nolans Bore rare-earth element-phosphorus-uranium mineral system: geology, origin and post-depositional modifications. Miner Depos 51(6):797–822

Jiang SY, Wang RC, Xu XS, Zhao KD (2005) Mobility of high field strength elements (HFSE) in magmatic-, metamorphic-, and submarine-hydrothermal systems. Phys Chem Earth 30:1020–1029

Johnson SP, Sheppard S, Rasmussen B, Wingate MTD, Kirkland CL, Muhling JR, Fletcher IR, Belousova EA (2011) Two collisions, two sutures: punctuated pre-1950 Ma assembly of the West Australian Craton during the Ophthalmian and Glenburgh Orogenies. Precambr Res 189(3–4):239–262

Johnson SP, Thorne AM, Tyler IM, Korsch RJ, Kennett BLN, Cutten HN, Goodwin J, Blay O, Blewett RS, Joly A, Dentith MC, Aitken ARA, Holzschuh J, Salmon M, Reading A, Heinson G, Boren G, Ross J, Costelloe RD, Fomin T (2013) Crustal architecture of the Capricorn Orogen, Western Australia and associated metallogeny. Aust J Earth Sci 60(6–7):681–705

Keller J (1989) Extrusive carbonatites and their significance. In: Bell K (ed) Carbonatites: Genesis and Evolution. Unwyn Hyman, London, pp 70–88

Keller J, Hoefs J (1995) Stable isotope characteristics of recent natrocarbonatites from Oldoinyo Lengai. In: Bell K, Keller J (eds) Carbonatite Volcanism. Springer, Berlin, pp 113–123

Kogarko LN, Suddaby P, Watkins P (1997) Geochemical evolution of carbonatite melts in Polar Siberia. Geochem Int 35:113–118

Kono Y, Kenney-Benson C, Hummer D, Ohfuji H, Park C, Shen G, Wang Y, Kavner A, Manning CE (2014) Ultralow viscosity of carbonate melts at high pressures. Nat Commun 5:5091

Krasnova NI, Petrov TG, Balaganskaya EG, Garcia D, Moutte J, Zaitsev AN, Wall F (2004) Introduction to phoscorites: occurrence, composition, nomenclature and petrogenesis. In: Wall F, Zaitsev AN (eds) Phoscorites and carbonatites from mantle to mine: the key example of the Kola Alkaline Province. The Mineralogical Society of Great Britain and Ireland, London, pp 45–74

Le Bas MJ (1977) Carbonatite-nephelinite volcanism. Wiley, London

Le Bas MJ (1989) Diversification of carbonatite. In: Bell K (ed) Carbonatites genesis and evolution. Unwin Hyman Ltd, London, pp 428–447

Le Maitre RW (2002) Igneous Rocks: a classification and glossary of terms: recommendations of international union of geological sciences, subcommission on the systematics of igneous rocks. Cambridge University Press, Cambridge

Martin DM, Thorne AM (2004) Tectonic setting and basin evolution of the Bangemall Supergroup in the northwestern Capricorn Orogen. Precambr Res 128(3):385–409

McDonough WF, Ss Sun (1995) The composition of the Earth. Chem Geol 120(3–4):223–253

Mitchell RH (1979) The alleged kimberlite-carbonatite relationship: additional contrary mineralogical evidence. Am J Sci 279:570–589

Motoyoshi Y, Hensen BJ (2001) F-rich phlogopite stability in ultrahigh-temperature metapelites from the Napier Complex, East Antarctica. Am Miner 86:1404–1413

Nelson DR, McCulloch MT, Sun S-S (1986) The origins of ultrapotassic rocks as inferred from Sr, Nd and Pb isotopes. Geochim Cosmochim Acta 50(2):231–245

Nicholls J, Carmichael JSE (1969) Peralkaline acid liquids: a petrological study. Contrib Miner Metrol 20:268–294

Occhipinti SA, Sheppard S, Passchier C, Tyler IM, Nelson DR (2004) Palaeoproterozoic crustal accretion and collision in the southern Capricorn Orogen: the Glenburgh Orogeny. Precambr Res 128(3–4):237–255

Pearson JM (1996) Alkaline rocks of the Gifford Creek Complex, Gascoyne Province, Western Australia: their petrogenetic and tectonic significance. University of Western Australia

Pearson JM, Taylor WR (1996) Mineralogy and geochemistry of fenitized alkaline ultrabasic sills of the Gifford Creek Complex, Gascoyne Province, Western Australia. Can Miner 34:201–219

Pearson JM, Taylor WR, Barley ME (1996) Geology of the alkaline Gifford Creek Complex, Gascoyne Complex, Western Australia. Aust J Earth Sci 43(3):299–309

Petersen EU, Essene EJ, Peacor DR, Valley JW (1982) Fluorine endmember micas and amphiboles. Am Miner 67:538–544

Pilet S, Hernandez J, Sylvester P, Poujol M (2005) The metasomatic alternative for ocean island basalt chemical heterogeneity. Earth Planet Sci Lett 236(1):148–166

Pirajno F (2015) Intracontinental anorogenic alkaline magmatism and carbonatites, associated mineral systems and the mantle plume connection. Gondwana Res 27:1181–1216

Pirajno F, González-Álvarez I (2013) The ironstone veins of the Gifford Creek ferrocarbonatite complex, Gascoyne Province: Geological Survey of Western Australia, Record 2013/12. p 19

Pirajno F, González-Álvarez I, Chen W, Kyser KT, Simonetti A, Leduc E, leGras M (2014) The Gifford Creek Ferrocarbonatite Complex, Gascoyne Province, Western Australia: associated fenitic

alteration and a putative link with the ~ 1075 Ma Warakurna LIP. Lithos 202–203:100–119
Pisarevsky SA, Wingate MTD, Li Z-X, Wang X-C, Tohver E, Kirkland CL (2014) Age and paleomagnetism of the 1210 Ma Gnowangerup-Fraser dyke swarm, Western Australia, and implications for late Mesoproterozoic paleogeography. Precambr Res 246:1–15
Prokopyev IR, Borisenko AS, Borovikov AA, Pavlova GG (2016) Origin of REE-rich ferrocarbonatites in southern Siberia (Russia): implications based on melt and fluid inclusions. Miner Pet 110(6):845–859
Reguir EP, Chakhmouradian AR, Halden NM, Malkovets VG, Yang P (2009) Major- and trace-element compositional variation of phlogopite from kimberlites and carbonatites as a petrogenetic indicator. Lithos 112:372–384
Rubin JN, Henry CD, Price JG (1993) The mobility of zirconium and other "immobile" elements during hydrothermal alteration. Chem Geol 110:29–47
Russel HD, Hiemstra SA, Groenevelf D (1954) The mineralogy and petrology of the carbonatite at Loolekop, Eastern Transvaal. Trans Geol Soc S Afr 57:197–208
Sallet R (2000) Fluorine as a tool in the petrogenesis of quartz-bearing magmatic associations: applications of an improved F-OH biotite–apatite thermometer grid. Lithos 50(1):241–253
Salvi S, Williams-Jones AE (1996) The role of hydrothermal processes in concentrating high-field strength elements in the Strange Lake peralkaline complex, northeastern Canada. Geochim Cosmochim Acta 60:1917–1932
Sheppard S, Occhipinti SA, Nelson DR (2005) Intracontinental reworking in the Capricorn Orogen, Western Australia: the 1680-1620 Ma Mangaroon Orogeny. Aust J Earth Sci 52(3):443–460
Sheppard S, Bodorkos SP, Johnson SP, Wingate MTD, Kirkland CL (2010) The Paleoproterozic Capricorn Orogeny: intracontinental reworking not continent-continent collision. Geological Survey of Western Australia, Report 108, p 33
Simonetti A, Bell K (1994) Isotopic and geochemical investigation of the Chilwa Island Carbonatite Complex, Malawi: evidence for a depleted mantle source region, liquid immiscibility, and open system behaviour. J Petrol 35:1597–1621
Slezak P (2019) Petrology of the Gifford Creek Carbonatite Complex and the Yangibana LREE district, Western Australia: new insights from isotope geochemistry and geochronology. Phd Thesis, James Cook University, Townsville
Slezak P, Spandler C (2019) Carbonatites as recorders of mantle-derived magmatism and subsequent tectonic events: an example of the Gifford Creek Carbonatite Complex, Western Australia. Lithos 328–329:212–227
Slezak P, Spandler C, Blake K (2018) Ghosts of apatite past: using hyperspectral cathodoluminescence and micro-geochemical data to reveal multi-generational apatite in the Gifford Creek Carbonatite Complex, Australia. Can Mineral 56:773–797
Smith CB (1983) Pb, Sr and Nd isotopic evidence for sources of southern African Cretaceous kimberlites. Nature 304(5921):51–54
Spandler C, Morris C (2016) Geology and genesis of the Toongi rare metal (Zr, Hf, Nb, Ta, Y and REE) deposit, NSW, Australia, and implications for rare metal mineralization in peralkaline igneous rocks. Contrib Miner Petrol 171(12):104
Ss Sun, McDonough WF (1989) Chemical and isotopic systematics of oceanic basalts: implications for mantle composition and processes. In: Saunders AD, Norry MJ (eds) Magmatism in the ocean basins, vol 42. Geological Society Special Publication, London, pp 313–345
Stracke A (2012) Earth's heterogeneous mantle: a product of convection-driven interaction between crust and mantle. Chem Geol 330–331:274–299
Stracke A, Hofman AW, Hart SR (2005) FOZO, HIMU, and the rest of the mantle zoo. Geochem Geophys Geosyst 6:1–20
Tao R, Fei Y, Zhang L (2013) Experimental determination of siderite stability at high pressure. Am Miner 98:1565–1572
Taylor HP, Frechen J, Degens E (1967) Oxygen and carbon isotope studies of carbonatites from the Laacher See District, West Germany and the Alno District, Sweden. Geochim Cosmochim Acta 31:407–430
Thompson RN, Smith PM, Gibson SA, Mattey DP, Dickin AP (2002) Ankerite carbonatite from Swartbooisdrif, Namibia: the first evidence for magmatic ferrocarbonatite. Contrib Miner Petrol 143:377–395
Timofeev A, Migdisov AA, Williams-Jones AE (2015) An experimental study of the solubility and speciation of niobium in fluoride-bearing aqueous solutions at elevated temperature. Geochim Cosmochim Acta 158:103–111
Vartiainen H (1980) The petrography, mineralogy and petrochemistry of the Sokli carbonatite massif, northern Finland. In: Bulletin, 313. Geological Survey of Finland, p 126
Veizer J, Ala D, Azmy K, Bruckschen P, Buhl D, Bruhn F, Carden GAF, Diener A, Ebneth S, Godderis Y, Jasper T, Korte C, Pawellek F, Podlaha OG, Strauss H (1999) 87Sr/86Sr, δ13C and δ18O evolution of Phanerozoic seawater. Chem Geol 161(1):59–88
Veksler IV, Nielsen TFD, Sokolov SV (1998) Mineralogy of crystallized melt inclusions from Gardiner and Kovdor ultramafic alkaline complexes: implications for carbonatite genesis. J Petrol 39(11–12):2015–2031
Wall F, Zaitsev AN (2004) Rare earth metals in Kola carbonatites. In: Wall F, Zaitsev AN (eds) Phoscorites and carbonatites from mantle to mine: the key example of the kola alkaline province. The Mineralogical Society of Great Britain and Ireland, Cambridge, pp 341–373
Watson EB (1979) Zircon saturation in felsic liquids: experimental results and applications to trace element geochemistry. Contrib Miner Metrol 70:407–419
Woolley AR (1982) A discussion of carbonatite evolution and nomenclature, and the generation of sodic and potassic fenites. Miner Mag 46(338):13–17
Woolley AR, Bailey DK (2012) The crucial role of lithospheric structure in the generation and release of carbonatites: geological evidence. Miner Mag 76(2):259–270
Woolley AR, Buckley HA (1993) Magnesite-siderite series carbonates in the Nkombwa and Newania carbonatite complexes. S Afr J Geol 96:126–130
Woolley AR, Church AA (2005) Extrusive carbonatites: a brief review. Lithos 85:1–14
Woolley AR, Kempe DRC (1989) Carbonatites: nomenclature, average chemical compositions, and element distribution. In: Bell K (ed) Carbonatites genesis and evolution. Unwin Hyman Ltd, London, pp 1–14
Woolley AR, Kjarsgaard BA (2008) Paragenetic types of carbonatite as indicated by the diversity and relative abundances of associated silicate rocks: evidence from a global database. Can Miner 46:741–752
Workman RK, Hart SR, Jackson M, Regelous M, Farley KA, Blusztajn J, Kurz M, Staudigel H (2004) Recycled metasomatized lithosphere as the origin of Enriched Mantle II (EM2) end-member: evidence from the Samoan Volcanic Chain. Geochem Geophys Geosyst 5:1–44
Wyllie PJ (1965) Melting relationships in the system CaO–MgO–CO_2–H_2O, with petrological applications. J Petrol 6:101–123
Yaxley G, Ghosh S, Kiseeva K, Mallik A, Spandler C, Thomson A, Walter M (2019) Chapter 6. CO_2-rich melts in the Earth. In: Orcutt B, Daniel I, Dasgupta R (eds) Whole earth carbon: past and present. Cambridge University Press, pp 129–162

Yuhara M, Hirahara Y, Nishi N, Kagami H (2005) Rb–Sr, Sm–Nd ages of the phalaborwa carbonatite complex, South Africa. Polar Geosci 18:101–113

Zaitsev AN, Bell K (1995) Sr and Nd isotope data of apatite, calcite and dolomite as indicators of source, and the relationships of phoscorites and carbonatites from the Kovdor massif, Kola peninsula, Russia. Contrib Miner Petrol 121:324–335

Zaitsev AN, Sitnikova MA, Subbotin VV, Fernandez-Suarez J, Jeffries TE (2004) Sallanlatvi complex—a rare example of magnesite and siderite carbonatites. In: Wall F, Zaitsev AN (eds) Phoscorites and carbonatites from mantle to mine: the key example of the Kola Alkaline Province. Geological Society of Great Britain & Ireland, London, pp 201–245

Zi JW, Gregory C, Rasmussen B, Sheppard S, Muhling JR (2017) Using monazite geochronology to test the plume model for carbonatites: the example of Gifford Creek Carbonatite Complex, Australia. Chem Geol 463:50–60

Zurevinski SE, Mitchell RH (2011) Highly evolved hypabyssal kimberlite sills from Wmindji, Quebec, Canada: insights into the process of flow differentiation in kimberlite magmas. Contrib Miner Petrol 161:765–776